UNIMORE
UNIVERSITÀ DEGLI STUDI DI
MODENA E REGGIO EMILIA

UNIVERSITY OF MODENA AND REGGIO EMILIA

DEPARTMENT OF LIFE SCIENCES

Master's Degree in

Pharmaceutical Chemistry and Technology

Development and optimization of polymer-based monolithic capillary columns for micro-HPLC analyses

Relator:

Prof. Cecilia Rustichelli

University of Modena and Reggio Emilia

Co-relator:

Doc. Ing. Petr Cesla, Ph.D.

University of Pardubice

Experimental Thesis by

Chiara Anghinolfi

Academic Year 2024/2025

Abstract

The transition toward capillary liquid chromatography (micro-HPLC) represents a fundamental response to the requirements of modern "green" analytical chemistry, enabling high sensitivity in volume-limited samples and a drastic reduction in solvent consumption. Compared to conventional packed columns, polymeric monolithic supports offer an interconnected network of macropores that ensures high hydrodynamic permeability. However, the analysis of complex biological matrices requires stationary phases capable of resolving analytes with widely varying polarities. Clinical monitoring of acetaminophen is hindered by the need to simultaneously separate the parent molecule from its highly hydrophilic metabolites, a challenge that requires precise molecular engineering of the polymeric matrix.

This experimental thesis focused on the synthesis and characterization of a library of nine monolithic columns to identify the correlation between chemical structure and chromatographic performance. To validate their structural integrity and efficiency, a preliminary kinetic characterization was conducted analyzing a homologous series of alkylbenzenes. This approach was aimed to evaluate the overall system response in terms of chromatographic band broadening (hydrodynamic stress-test), rather than to enable the qualitative identification of individual components. It also allowed the exclusion of potentially morphologically unstable matrices before proceeding to the analysis of polar metabolites.

The results highlighted distinct trends for each cross-linker class:

- Glycol Series (Ethylene glycol dimethacrylate (EDMA), Triethylene glycol dimethacrylate (TriEDMA), Tetraethylene glycol dimethacrylate (TeEDMA)): structural homogeneity improved with increasing oxyethylene chain length. TeEDMA exhibited the best kinetic efficiency and low HETP (Height Equivalent to a Theoretical Plate) values.
- Aliphatic Series (Butane-1,3-diol dimethacrylate (1,3-BUDMA), Tetramethylene dimethacrylate (1,4-BUDMA), Hexamethylene dimethacrylate (HEDMA), Decane-1,10-diol dimethacrylate (DeEDMA)): the use of alkyl spacers generated less organized structures; as hydrophobicity increased (C6 and C10 chains), a deterioration in mass transfer was observed for small molecules. 1,4-BUDMA

proved to be an enigmatic case, showing oversized macropores and kinetic instability despite low theoretical HETP values.

- Aromatic and Multifunctional Series (1,4-Phenylene dimethacrylate (PhDMA), Pentaerythritol triacrylate (PETRA)): these led to structural failures such as detachment from the capillary wall (wall-effect) or incoherent and fractured networks.

Based on these results, TeEDMA, TriEDMA, and 1,4-BUDMA columns were selected for the separation of acetaminophen and its main polar metabolites: acetaminophen-cysteine, acetaminophen-N-acetylcysteine, and acetaminophen-glutathione. Final tests confirmed the superiority of the TeEDMA stationary phase, which exhibited stronger and more stable interactions with polar conjugates. In a future perspective, the optimization of the elution gradient and the ionic strength of the mobile phase will allow these prototypes to be transformed into advanced diagnostic tools. The modulation of the cross-linker chain is confirmed as a key strategy for engineering next-generation monolithic stationary phases, paving the way for integrated microfluidic systems for point-of-care therapeutic monitoring and high-resolution, rapid bioanalytical analysis.

Riassunto Analitico

La transizione verso la cromatografia liquida capillare (micro-HPLC) rappresenta una risposta fondamentale alle esigenze della moderna chimica analitica "green", permettendo un'elevata sensibilità in campioni a volume limitato e una drastica riduzione del consumo di solventi. Rispetto alle colonne impaccate convenzionali, i supporti monolitici polimerici offrono una rete interconnessa di macropori che garantisce un'elevata permeabilità idrodinamica. Tuttavia, l'analisi di matrici biologiche complesse richiede fasi stazionarie capaci di risolvere analiti con polarità molto diverse. Il monitoraggio clinico del paracetamolo è reso difficile dalla necessità di separare simultaneamente la molecola madre dai suoi metaboliti altamente idrofili, sfida che richiede una progettazione molecolare precisa della matrice polimerica.

La presente tesi sperimentale si è concentrata sulla sintesi e sulla caratterizzazione di una libreria di nove colonne monolitiche per identificare la correlazione tra struttura chimica e prestazioni cromatografiche. Per valutarne l'integrità strutturale e l'efficienza, è stata condotta una caratterizzazione cinetica preliminare mediante l'analisi di una serie omologa di alchilbenzeni allo scopo di valutare la risposta complessiva del sistema in termini di allargamento delle bande cromatografiche (hydrodynamic stress test), piuttosto che l'identificazione qualitativa dei singoli componenti. Inoltre, ha consentito di escludere le matrici potenzialmente instabili dal punto di vista morfologico prima di procedere all'analisi dei metaboliti polari.

I risultati hanno evidenziato andamenti distinti per ogni classe di cross-linker:

- Serie Glicolica (Ethylene glycol dimethacrylate (EDMA), Triethylene glycol dimethacrylate (TriEDMA), Tetraethylene glycol dimethacrylate (TeEDMA)): l'omogeneità strutturale migliora con l'aumento della lunghezza della catena ossietilenica. TeEDMA ha mostrato la migliore efficienza cinetica e bassi valori di HETP (*Height Equivalent to a Theoretical Plate*).
- Serie Alifatica (Butane-1,3-diol dimethacrylate (1,3-BUDMA), Tetramethylene dimethacrylate (1,4-BUDMA), Hexamethylene dimethacrylate (HEDMA), Decane-1,10-diol dimethacrylate (DeEDMA)): l'uso di spacer alchilici ha generato strutture meno organizzate e all'aumentare dell'idrofobicità (catene C6 e C10) è stato osservato un deterioramento del trasferimento di massa per molecole di piccole

dimensioni. Il 1,4-BUDMA è risultato enigmatico, mostrando macropori sovradimensionati e instabilità cinetica nonostante bassi valori teorici di HETP.

- Serie Aromatiche/Multifunzionali (1,4-Phenylene dimethacrylate (PhDMA), Pentaerythritol triacrylate (PETRA)): hanno mostrato difetti strutturali quali distacchi dalla parete (wall-effect) o formazione di reti incoerenti e fratturate.

Sulla base dei risultati ottenuti, le colonne TeEDMA, TriEDMA e 1,4-BUDMA sono state selezionate per la separazione del Paracetamolo e dei suoi principali metaboliti polari: acetaminofene-cisteina, acetaminofene-N-acetilcisteina e acetaminofene-glutatione. I test finali hanno confermato la superiorità della fase stazionaria TeEDMA, capace di stabilire un'interazione più forte con i coniugati polari. In una prospettiva futura, l'ottimizzazione del gradiente di eluizione e della forza ionica della fase mobile permetterà di trasformare questi prototipi in strumenti diagnostici avanzati. La modulazione della catena del cross-linker si conferma lo strumento principale per ingegnerizzare fasi stazionarie monolitiche di nuova generazione, aprendo la strada a sistemi micro-fluidici integrati per il monitoraggio terapeutico "point-of-care" e analisi bioanalitiche rapide ad alta risoluzione.

Index

1. Introduction

1.1 Evolution and Design of Polymeric Monolithic Stationary Phases

1.1.1 The Need: From Packed to Monolithic Beds

The analytical challenges posed by complex biological matrices and miniaturized sampling require stationary phases that combine high selectivity with excellent hydrodynamic properties. In this context, polymeric monolithic columns have emerged as leading technology in capillary liquid chromatography to meet these needs [1,2]. The transition towards capillary-scale liquid chromatography (micro-HPLC) is primarily driven by the necessity for enhanced sensitivity in volume-limited samples and the reduction of solvent consumption, adhering to the principles of "Green Analytical Chemistry" [3]. However, conventional packed-bed columns face significant physical limitations when miniaturized into capillary formats with an internal diameter (ID) of 320 µm.

The most critical hurdle is the hydrodynamic resistance. In a column packed with discrete particles, the backpressure (ΔP) is described by the Kozeny-Carman equation, derived from Darcy's Law [4]:

$$\Delta P = = \frac{\eta \cdot u \cdot L \cdot \Phi}{d_p^2}$$

where η is the mobile phase viscosity, u is the linear velocity, L is the column length, and d_p is the particle diameter. As shown in **Figure 1**, the ordered arrangement of these isolated spherical particles creates a dense bed where the mobile phase must navigate through narrow interstitial spaces, leading to high flow resistance. Furthermore, packed capillary columns require the use of retaining frits to keep the stationary phase in place; these frits are often the primary cause of clogging, dead volume, and peak broadening in micro-scale separations [5].

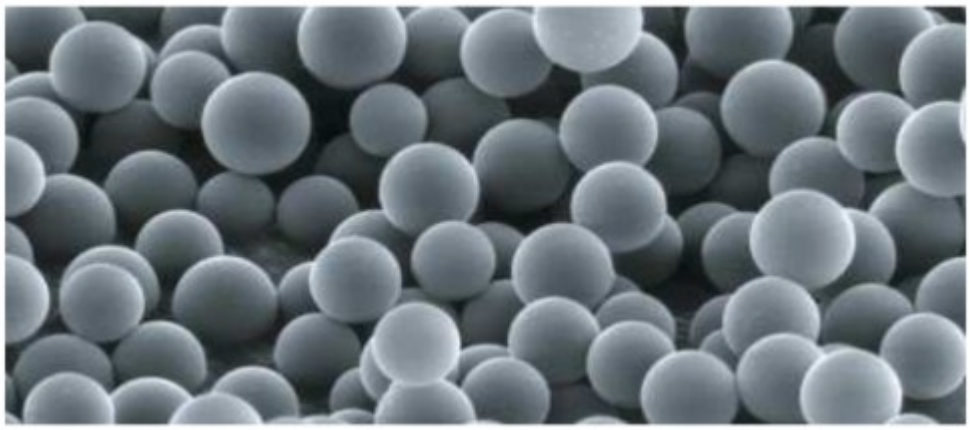

Figure 1: Conceptual SEM image of a conventional packed bed stationary phase. *The ordered arrangement of spherical, monodisperse porous particles creates significant flow resistance, necessitating elevated backpressures for mobile phase flow. Modified from internal documents, courtesy of Prof. P. Cesla.*

A monolithic HPLC column is prepared *in situ* by generating a continuous porous structure directly inside the column tube through a controlled polymerization or sol–gel process. Unlike conventional columns, which are packed with discrete particles, a monolithic column consists of a single, continuous piece of porous material, typically silica or polymer. This structure is characterized by a bimodal pore network: large through-pores (macropores, pore size >1 μm) that enable high permeability and low backpressure, and smaller pores (mesopores, 2–50 nm) that provide a high surface area for analyte interactions, promoting efficient mass transfer.

This unique architecture results in a rigid, homogeneous, and highly interconnected structure that is firmly anchored to the column walls. The morphology of monolithic supports is clearly visible via **Scanning Electron Microscopy (SEM)**, as shown in **Figure 2**, highlighting the contrast with conventional columns, where the stationary phase is composed of a packed bed of individual spherical particles. The combination of convective macropores and mesopores not only drastically reduces system backpressure but also improves chromatographic efficiency for small molecules [5,7].

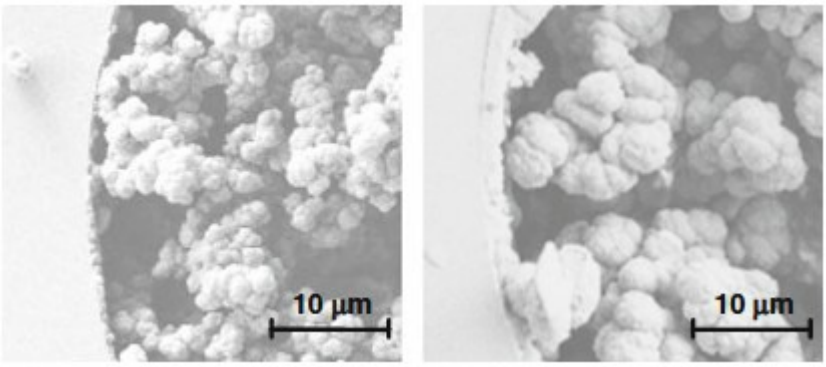

Figure 2: Scanning Electron Microscopy (SEM) investigation of the polymethacrylate monolithic support. *(a) Cross-section of the capillary showing the perfect adherence of the polymer matrix to the internal walls; (b) High-magnification detail highlighting the globular morphology and the interconnected flow-through macropores. Scale bars are provided for size comparison (Adapted from Nischang et al., 2010) [6].*

Historically, organic polymer monoliths were primarily utilized for the separation of large biomolecules due to their large through-pores and perceived limited surface area [7]. However, recent advancements have demonstrated their high potential for small molecule separations by precisely tailoring the polymerization conditions to enhance mesoporosity and surface chemistry [6,8]. This evolution has made them a competitive tool for the rapid kinetic screening of pharmaceutical compounds like acetaminophen, where high throughput and efficiency are required [9]. The ability to engineer the polymer matrix at the molecular level, specifically through the selection of specialized cross-linkers, allows for the creation of tailor-made stationary phases capable of resolving complex mixtures in miniaturized HPLC systems.

1.1.2 Chemistry: Synthesis and Pore Architecture

A monolith is defined as a single, continuous block of porous material synthesized in situ within 320 µm ID capillary through a polymerization process involving monomers, cross-linkers, and porogenic solvents [1]. The flexibility of this approach allows for an amazingly wide variety of chemistry and techniques enabling the preparation of tailor-made columns where the morphology is optimized for specific applications [1,2].

The synthesis of these materials generally follows three main strategies: in situ organic polymerization, the sol-gel process for silica-based monoliths, and the development of hybrid organic-silica monoliths [5]. For the purposes of this research, the in situ radical polymerization of organic monomers was chosen. This strategy offers the highest degree of flexibility, allowing for the synthesis of "tailor-made" columns where the morphology and

chemistry are precisely optimized for specific applications by tuning the monomer-to-porogen ratio [1,7]. In particular, methacrylate-based monoliths are characterized by a bimodal pore structure. This architecture includes large through-pores (macropores), which ensure high permeability and low resistance to the mobile phase flow, and mesopores, which provide the high surface area necessary for solute interaction and retention [5,10].

Surface Functionalization: Pre-treatment, Etching and Silanization

To implement the chosen in situ organic approach, the inner surface of the fused-silica capillary must be chemically modified. This ensures that the monolithic bed remains covalently anchored to the wall, preventing extrusion under high pressure. According to established protocols [9,11], the procedure involves several critical stages:

1. Pre-treatment and Activation (Etching) (**Figure 3**): The capillary undergoes an initial rinsing cycle with acetone and distilled water to remove any organic residues and ensure uniform surface wettability. Subsequently, an alkaline etching step with sodium hydroxide (NaOH) is performed. This treatment promotes the hydrolysis of siloxane bridges (Si-O-Si), breaking the stable silica network to increase the density of reactive sites. Although this step leaves the surface in a deprotonated, negatively charged state ($Si - O^-$), its primary purpose is to "corrode" the top molecular layer, effectively increasing the potential silanol density. A subsequent wash with hydrochloric acid (HCl) ensures the complete protonation of these sites into active silanol groups (Si-OH). This sequential basic-acidic treatment transforms a relatively inert surface into a densified "forest" of reactive hydroxyl groups, which is essential for ensuring a high-density covalent anchoring of the subsequent organic layer. A final rinse with ethanol prepares the surface for the organic functionalization.

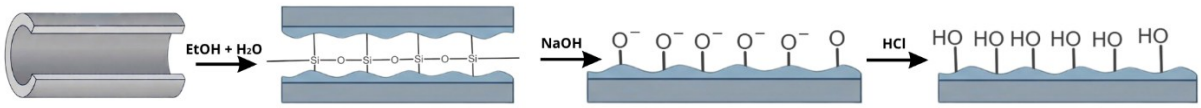

Figure 3: Schematic representation of the capillary surface activation process*. Initial cleaning with an aqueous-ethanol solution, followed by alkaline treatment to cleave siloxane bridges, and final protonation with HCl to expose the silanol groups. Created with Canva.*

2. Silanization (**Figure 4**): The activated surface is then reacted with a silanizing solution containing 3-(trimethoxysilyl)propyl methacrylate in ethanol. During this phase, the methoxy groups of the silanizing agent undergo a condensation reaction with the surface silanols, forming stable siloxane bonds. After the reaction, the capillary is rinsed with ethanol and dried under a stream of nitrogen. A 24-hour equilibration period at room temperature follows to ensure the complete formation and stability of the covalent bridge between the inorganic silica wall and the methacrylate functionalities.

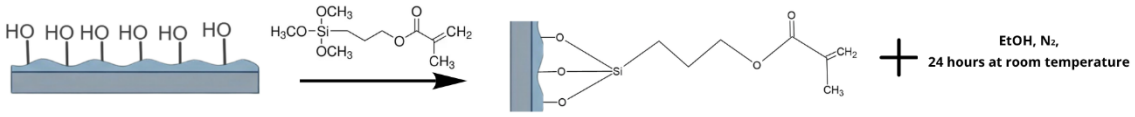

Figure 4: Surface modification of the activated silica capillary. *Covalent attachment of methacrylate-terminated silane groups to the inner surface to enable subsequent surface-initiated radical polymerization. Created with Canva.*

Monolithic Mixture and Polymerization Mechanism

Once the capillary surface is fully activated and silanized, the monolithic bed is synthesized through a single-step Free Radical Polymerization (FRP). Unlike traditional packing methods, the entire structure is formed in situ from a homogeneous polymerization mixture[7,9]. This mixture is composed of:

- Functional Monomers: These determine the final surface chemistry and the retention mechanisms of the column.
- Cross-linking Monomers: These act as the structural "architects" of the monolith. The cross-linker interconnects the growing polymer chains into a rigid, non-swelling three-dimensional scaffold [12]. This rigidity is fundamental to ensure that the porous properties remain stable during polymerization and that the matrix does not collapse under the LC operative pressure.
- Porogenic Solvents: A balanced mixture of solvents that remains inert during the reaction but dictates the final morphology. The selection of the porogenic solvent system, specifically the ratio between a solvating agent (1-propanol) and a non-solvating co-porogen agent (1,4-butanediol), is the most effective tool for tuning the column's permeability and surface area [9].
- Initiator: A thermally unstable compound, such as azobisisobutyronitrile (AIBN), which is dissolved directly into the monomer/porogen mix.

The polymerization process follows the classical mechanism of radical chain growth (**Figure 5**), evolving through three distinct kinetic stages:

- Initiation: The process is triggered by the thermal decomposition of the AIBN initiator. Upon reaching its decomposition temperature, the initiator undergoes homolytic cleavage, releasing nitrogen gas and generating reactive cyanoisopropyl radicals. These radicals immediately attack the vinyl groups of the methacrylate monomers, creating the first active centers.
- Propagation: As the reaction enters this phase, the polymer chains grow rapidly and branch out due to the presence of the cross-linking agents. During this stage the Reaction-Induced Phase Separation (RIPS) occurs: the 1-propanol maintains the initial homogeneity, while the 1,4-butanediol (acting as a poor solvent) triggers a controlled phase separation as the molecular weight increases. This forces the growing chains to aggregate into microglobules, creating the interconnected macropores necessary for the high flow characteristics [9,12].
- Termination: The process concludes when the growth stops, either by the combination of two radicals or by their quenching. This leaves a continuous, bimodal porous scaffold that is chemically stable across the entire pH spectrum (pH 1–14).

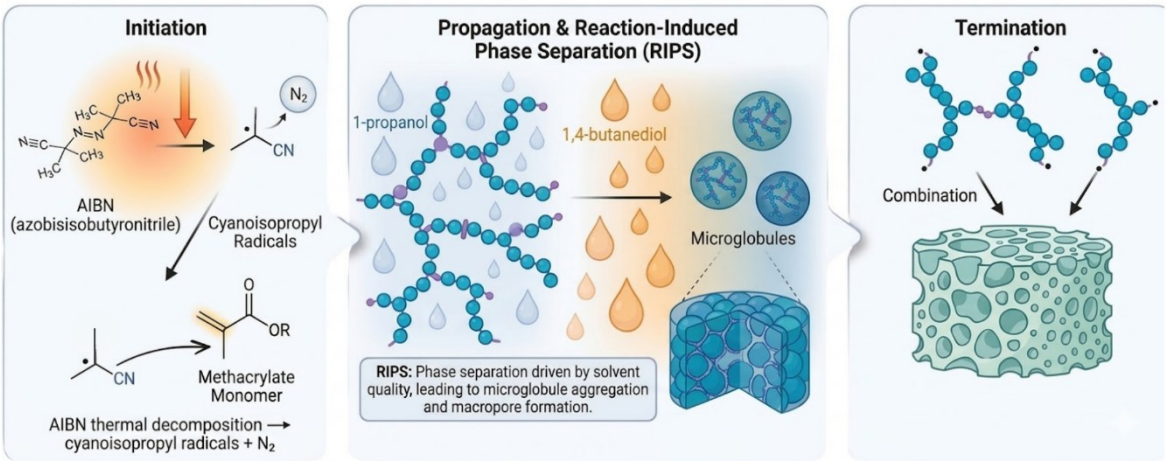

Figure 5: Schematic overview of the in-situ polymerization process for porous monolith formation. *(Left) Thermal initiation of AIBN generating cyanoisopropyl radicals, which react with a methacrylate monomer. (Center) Propagation and Reaction-Induced Phase Separation (RIPS) mechanism driven by the decreasing solubility of the growing polymer in the ternary solvent mixture (monomer, 1-propanol, 1,4-butanediol), leading to microglobule aggregation. (Right) Chain termination by combination and final aggregation of microglobules to form the macroporous monolithic structure. Created with Canva.*

1.1.3 Kinetic Evaluation and the Van Deemter Equation

While polymeric monoliths offer significant structural and chemical advantages, achieving high efficiency for the separation of small molecules, like acetaminophen and its metabolites, is more difficult than for large biomolecules. It has been highlighted in literature that the performance of organic polymer monoliths for small molecules is often limited by the lack of sufficient surface area and slow mass transfer in the stagnant mobile phase within the pores [1]. Small molecules require a very precise pore structure and a high surface area to improve mass transfer and prevent peak broadening [1,13].

In this context, the choice and concentration of the cross-linking agent are among the most critical factors. As shown in systematic studies on (poly)methacrylate monoliths, the chemical nature and the concentration of the cross-linking agent determine both the separation efficiency and the hydrophobic selectivity of the column Liquid Chromatography [8].

The chromatographic efficiency is traditionally described by the Van Deemter equation, which correlates the height equivalent to a theoretical plate (H) with the linear velocity of the mobile phase (u):

$$H = A + \frac{B}{u} + C \cdot u$$

In this model (**Figure 6**), the term A accounts for eddy diffusion, B for longitudinal diffusion, and C for the resistance to mass transfer. For organic polymer monoliths, the C-term is particularly significant when separating small molecules. As discussed in the literature regarding the quest for enhanced efficiency [5], slow diffusion into the polymer matrix can lead to a drastic decrease in performance at higher flow rates [13].

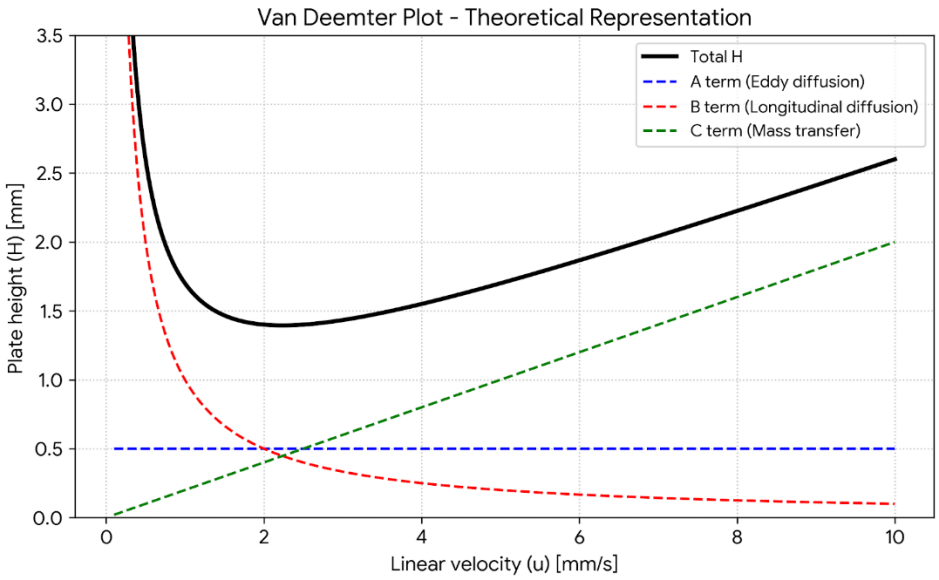

Figure 6: Theoretical Van Deemter plot for column efficiency characterization. *The graph illustrates the relationship between the height equivalent to a theoretical plate (H) and the mobile phase linear velocity (u). The total H curve (black line) results from the combination of the three primary sources of band broadening: Eddy diffusion (A term, blue), longitudinal diffusion (B term, red), and resistance to mass transfer (C term, green). The minimum of the curve represents the optimal linear velocity for maximum separation efficiency. (Data processed via Google Colab/Python)*

To better evaluate the kinetic performance, kinetic plots, such as the Poppe plot, can be employed to investigate the limits of the support in terms of analysis time and efficiency [14] (**Figure 7**).

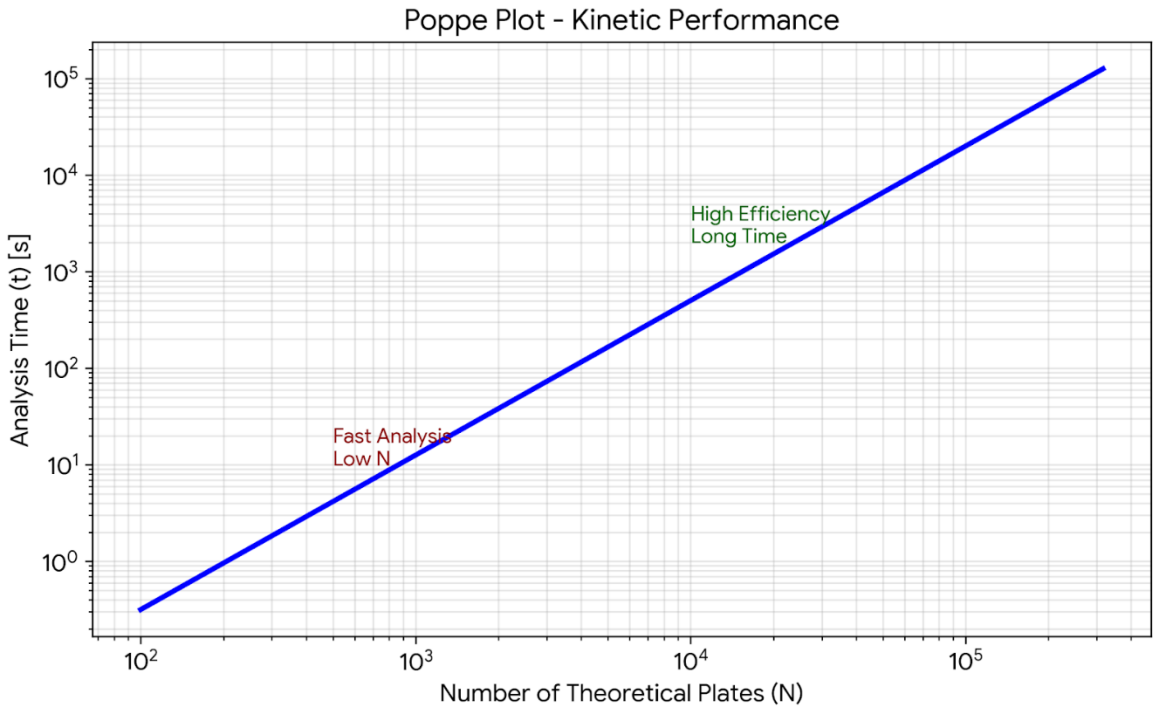

***Figure 7:* Kinetic performance evaluation via Poppe plot.** *The double-logarithmic scheme represents the correlation between the number of theoretical plates (N) and the required analysis time (t). This kinetic plot allows for the identification of the performance limits of the stationary phase, balancing the quest for high efficiency (large N) with the practical need for fast chromatographic separations in miniaturized systems [14].*

Beyond the evaluation of H, the characterization of capillary columns requires a rigorous analysis of the peak standard deviation expressed in terms of volume (σ_v). In miniaturized systems, even minimal extra-columns volumes can lead to significant peak broadening. This phenomenon is particularly critical in micro-HPLC, where the total volume of the capillary column is extremely small.

To evaluate the real impact of these dispersive effects, the volumetric peak dispersion (σ_v) is calculated by correlating the volumetric flow rate (F) and the peak dispersion in time (σ_t) through the relationship:

$$\sigma_v = F \cdot \sigma_t$$

By optimizing the cross-linking density and the porogenic mixture, it is possible to minimize these dispersive effects, ensuring high resolution for critical metabolic pairs while maintaining operative backpressures suitable for micro-HPLC applications [8,13]

1.1.4 Hydrodynamic Properties and Darcy's Law

The unique morphology of this support, characterized by a highly interconnected network of macropores, allows the mobile phase to pass through the column with minimal resistance. This bimodal porosity not only drastically reduces the system backpressure but also ensures that the monolithic bed remains stable even under high-flow conditions.

While the hydrodynamic resistance of particulate beds is traditionally described by the Kozeny-Carman equation, this model is not directly applicable to monolithic structures due to the absence of discrete particles (d_p)[4]. Instead, the flow behavior and permeability of the monolithic stationary phase are mathematically defined by Darcy's Law:

$$\Delta P = \frac{\eta \cdot L \cdot u}{K^0}$$

In this equation, ΔP is the pressure drop, η represents the mobile phase viscosity, L is the column length, and u is the linear velocity. The parameter K^0 is the specific permeability, a fundamental constant that reflects the structural quality of the monolith.

For the methacrylate-based monoliths synthesized in this work, K^0 is intrinsically linked to the size and interconnectivity of the macropores (flow-through channels) formed during the phase separation process. A high K^0 value is essential in micro-HPLC to maintain operative backpressures suitable for miniaturized instrumentation, while still allowing the rapid mass transfer necessary for the separation of small molecules like acetaminophen [6,10]. By precisely tailoring the porogenic mixture and the cross-linking density, it is possible to engineer a support that balances high permeability with optimal chromatographic efficiency.

1.2 Applications of Monolithic Columns in Liquid Chromatography

Historically, organic polymer monoliths were primarily utilized for the separation of large biomolecules due to their large through-pores and perceived limited surface area [1]. However, recent advancements have demonstrated their high potential for small molecule separations by precisely tailoring the polymerization conditions to enhance mesoporosity and surface chemistry [6,8]. The flexibility of this approach allows for an amazingly wide variety of chemistry and techniques enabling the preparation of tailor-made columns where morphology is optimized for specific applications [1,2].

1.2.1 From Biomolecules to Small Molecules: The Quest for Surface Area

The shift from analyzing large proteins to small pharmaceutical molecules required a fundamental change in how the monolithic scaffold is engineered. While large biomolecules interact mainly with the surface of the macropores, small molecules require access to a dense network of mesopores (2–50 nm) to achieve sufficient retention and resolution [13]. To make these materials competitive with traditional packed-bed columns, researchers have focused on:

- Increasing the Specific Surface Area: By optimizing the porogenic solvent ratio, it is possible to reduce the microglobule size, thereby increasing the area available for solute interaction [6].

- Enhancing Mass Transfer: The bimodal pore structure remains a key advantage, as it combines convective flow through macropores with efficient diffusion into the mesoporous layer, minimizing the resistance to mass transfer [10].

1.2.2 Selectivity and "Tailor-made" Chemistry

The ability to engineer the polymer matrix at the molecular level, specifically through the selection of specialized cross-linkers, allows for the creation of stationary phases capable of resolving complex mixtures in miniaturized HPLC systems. Unlike silica-based columns, which are often limited by the chemistry of silanization, polymeric monoliths offer a modular platform.

By varying the functional monomers and the chemical nature of the cross-linking agent is possible to finely tune the hydrophilicity, ion-exchange capacity, and specific selectivity of the support [8,9,15]. This systematic approach is essential for addressing the challenges of complex biological matrices, where a precise balance of interactions is needed to resolve analytes with widely different polarities [15].

The versatility of these tailor-made monolithic supports, specifically their ability to balance hydrophobic and hydrophilic interactions, is key in analyzing drugs with complex metabolic profiles [9]. A primary example of such a challenge is the monitoring of Acetaminophen (APAP) and its metabolites in biological matrices, where high-efficiency systems are required to resolve the parent drug from its more polar conjugates [10].

1.3 Acetaminophen

1.3.1 Background and Historical Overview

Acetaminophen (APAP), chemically designated as *N-(4-hydroxyphenyl) acetamide*, remains one of the most widely utilized non-opioid analgesic and antipyretic agents in modern medicine [16] (**Figure 8**). The molecule consists of a benzene ring core substituted by a hydroxyl group and an amide group (acetamide) in the (1,4) positions. It is the primary active ingredient analyzed in this study regarding its metabolic pathways and mechanisms of hepatotoxicity. Known globally as paracetamol, it serves as a cornerstone of pharmacological therapy, largely due to its favourable safety profile when compared to other classic analgesics [16]. The clinical history of the drug is marked by a series of pivotal discoveries by the late 19th century. While its antipyretic properties were first observed in 1887 by Harmon Northrop Morse, who synthesized the compound, its clinical introduction occurred later [17], in 1893, when Joseph von Mering introduced paracetamol as an alternative to phenacetin [18]. This work emerged from a broader scientific effort to develop effective antipyretics derived from aniline, a field that had gained significant momentum following the accidental discovery of the fever – reducing properties of acetanilide [18].

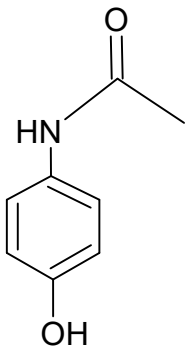

Figure 8: Chemical structure of Acetaminophen (N-acetyl-p-aminophenol, APAP).

The global success of APAP in pain management is primarily due to its superior gastrointestinal tolerability when compared to traditional non – selective non-steroidal anti-inflammatory drugs (NSAIDs) like aspirin [16,17]. While aspirin often is frequently associated with gastric mucosal injury and an increased risk of bleeding due to peripheral cyclooxygenase inhibition, APAP does not share these aggressive side effects [18,19]. This profile makes it a much safer alternative for patients with gastric sensitivities.

The adoption of APAP reached a peak in the 1980s following the documented link between aspirin and Reye's Syndrome [20]. This condition, characterized by acute encephalopathy

and hepatic metabolic decompensation, was observed in children recovering from viral infections who had taken aspirin [20]. Following public health warnings, aspirin virtually disappeared from paediatric prescriptions, cementing APAP as the gold standard for treating fever and pain in children [16,20].

Nevertheless, APAP safety profile remains valid only at therapeutic doses. Dose-dependent hepatotoxicity continues to be a major clinical concern, representing the main drawback of an otherwise highly manageable drug [16,18,21]. Despite these concerns, APAP has been considered the only safe analgesic during pregnancy for decades, as traditional NSAIDs are generally avoided due to their association with serious fetal complications, such as the premature closure of the ductus arteriosus.

This profile of APAP absolute safety has been recently challenged. Epidemiological evidence, highlighted in a 2021 international consensus statement [22], points toward a potential link between prolonged prenatal exposure and an increased risk of neurodevelopmental issues in children, including ADHD and autism spectrum disorders, as well as urogenital abnormalities. While the scientific community continues to debate these findings, the current clinical approach has shifted toward the precautionary principle. This means recommending that pregnant women use APAP only when strictly necessary, at the lowest effective dose, and for the shortest duration possible [18,22]. The reasons behind these potential adverse effects, as well as the drug's overall therapeutic efficacy, are deeply rooted in its unique biochemical behaviour. To better understand these clinical concerns, it is necessary to examine the underlying mechanisms of action and the complex metabolic pathways that characterize this molecule, which will be discussed in the following chapter.

1.3.2 Mechanism of Action

For decades, the pharmacological identity of APAP has been a paradox. Although it is often grouped with NSAIDs, it lacks their typical anti-inflammatory activity. This discrepancy stems from its distinctive interaction with cyclooxygenase (COX) enzymes, which differs fundamentally from that of traditional analgesics. While the therapeutic efficacy of APAP is well established, its precise mechanism of action has remained elusive, leading to its classification as an atypical analgesic that bridges the gap between peripherally acting drugs and central modulators [16,18].

To truly understand where the difference lies, it is necessary to examine the mechanism of action of traditional NSAIDs. As established by Vane and Botting [19], these drugs inhibit

the cyclooxygenase (COX) enzymes, which are responsible for catalyze the conversion of arachidonic acid into prostaglandins – the lipid mediators responsible for pain and inflammation.

A key point in their research is the distinction between two cyclooxygenase isoforms: COX-1, which is 'constitutive' and protects the stomach and kidneys, and COX-2, which is 'inducible' and upregulated during inflammation. Most classic drugs, like aspirin, are non-selective inhibitors that bind within a hydrophobic channel of the enzyme, thereby blocking prostaglandin synthesis. This mechanism underlies their strong anti-inflammatory efficacy but also explains their frequent gastrointestinal adverse effects: inhibition of COX-1 compromises the stomach's intrinsic protective mechanisms [19].

While the mechanism described by Vane and Botting [19] clearly explains how traditional NSAIDs work, it doesn't quite fit the clinical profile of APAP. Since APAP is a very weak inhibitor of both COX-1 and COX-2 in the presence of inflammation, researchers have begun to wonder if its primary target may lie elsewhere.

This uncertainty led to the hypothesis that a third, unidentified isoform could be responsible for the drug's effects. In 2002, Chandrasekharan et al. [23] seemed to find a potential explanation when they identified a variant of COX-1, which they named COX-3. This discovery was particularly interesting because, in canine models, COX-3 appeared to be highly sensitive to APAP, unlike the traditional COX-1 and COX-2 described previously.

The fact that COX-3 was found mainly in the cerebral cortex seemed to finally explain why the drug's action is so concentrated in the central nervous system. For several years, this was considered the most plausible explanation for the drug's 'central' nature. However, later studies showed that in humans, the COX-3 gene actually produces a different protein that doesn't seem to have the same functional role as in dogs.

In particular, when Schwab et al. [24] analyzed the human version of this gene, they found a major obstacle: while the variant exists in humans, it contains a frameshift mutation that is absent in dogs. This genetic difference means that in humans, the gene produces a truncated, non-functional protein. Consequently, Schwab and other researchers concluded that COX-3 could not be the functional target in humans, forcing the scientific community to look back at the original COX-1 and COX-2 enzymes, but from a different biochemical perspective: the interaction with the peroxidase (POX) site.

The shift back to investigating COX-1 and COX-2 led to the discovery that APAP's uniqueness lies not in which enzyme it targets, but in how it interacts with them. As demonstrated by Ouellet and Percival [21], COX enzymes are bifunctional, involving two distinct but coupled catalytic cycles: the peroxidase cycle and the cyclooxygenase cycle (**Figure 9**).

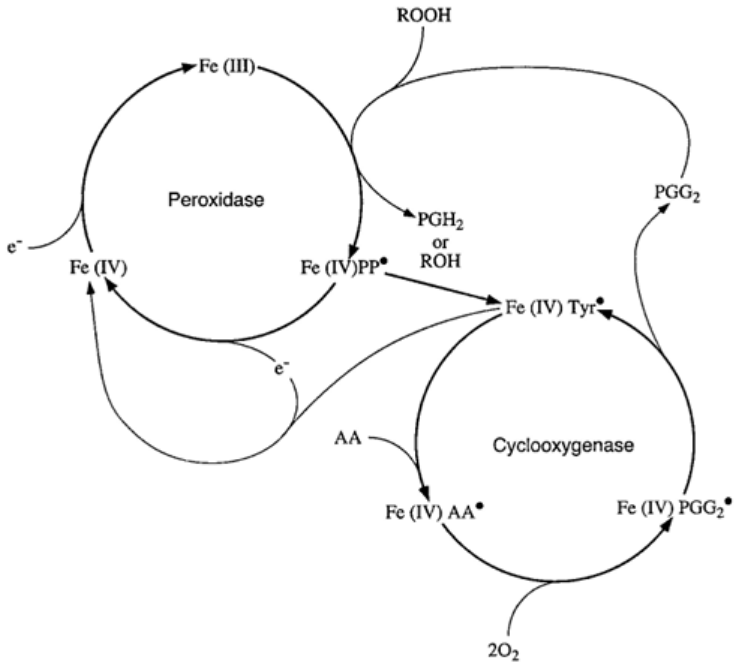

Figure 9 ***Catalytic mechanism of COX enzymes and acetaminophen inhibition.*** *The diagram illustrates the coupling between the peroxidase and cyclooxygenase cycles. Acetaminophen acts as a reducing agent, quenching the radical intermediates required for enzyme activation. Abbreviations:* $Fe(III)$*, resting state heme,* $Tyr\bullet$ *tyrosyl radical; AA, arachidonic acid; ROOH, hydroperoxides. Source*:[21].

To produce prostaglandins, the enzyme must first be 'activated' via the peroxidase cycle. This activation involves the oxidation of the heme group from its resting state ($Fe(III)$) to an intermediate state ($Fe(IV)$), which in turn generates a tyrosyl radical ($Tyr\bullet$). This radical is the essential 'spark' required to initiate the cyclooxygenase cycle by extracting a hydrogen atom from arachidonic acid.

APAP interferes with this process by acting as a reducing agent (or reducing co-substrate). Instead of blocking the cyclooxygenase channel like traditional NSAIDs, it donates electrons (e^-) to the peroxidase site. By doing so, it reduces the high-oxidation states of the heme and prevents the formation of the tyrosyl radical, effectively quenching the enzyme's activity before the prostaglandin synthesis can even begin [21].

This same biochemical mechanism explains why APAP is such an effective antipyretic. Fever is regulated by the hypothalamus, where the production of prostaglandins (specifically PGE2) acts as a signal to increase the body's temperature set-point.

Unlike inflamed joints or peripheral tissues, the brain environment has very low levels of hydroperoxides. In this 'low peroxide' environment, APAP's ability to act as a reducing agent remains intact. It can effectively quench the peroxidase activity of the COX enzymes in the central nervous system, reducing prostaglandin synthesis and thus lowering the fever. This confirms the drug's profile: it is a potent analgesic and antipyretic precisely because it excels in tissues where oxidative stress is minimal, while it remains ineffective where inflammation is high [16,18,21].

Despite the precision of the peroxidase inhibition theory, this mechanism may not fully explain the drug's total analgesic effect, particularly regarding its complex interaction with central pain pathways. This limitation has led researchers to explore non-prostaglandin related mechanisms, specifically involving the endocannabinoid system. Within the central nervous system, APAP acts as a prodrug; it undergoes deacetylation to *p-aminophenol*, which is subsequently conjugated with arachidonic acid by the enzyme Fatty Acid Amide Hydrolase (FAAH) to synthesize AM404 [17]. This metabolite enhances the body's endogenous antinociceptive tone by inhibiting the reuptake of anandamide and acting as a potent activator of TRPV1 (vanilloid) receptors in the spinal cord [16,17].

This dual action, enhancing endocannabinoid signalling and modulating vanilloid channels, provides a more comprehensive explanation for the drug's central analgesic properties. By bridging the gap between simple enzyme inhibition and complex neuromodulation, this pathway resolves much of the paradox traditionally associated with the drug's mechanism of action [16–18].

1.3.3 Metabolic Pathways and Mechanisms of Toxicity

The metabolism of APAP follows a dose-dependent pattern, where the drug's safety profile is determined by the metabolic disposition across competing pathways (**Figure 10**). In healthy adults, the maximum recommended therapeutic dose is typically 4 g per day [25]. APAP is also a classic example of a drug whose toxicity is not inherent to the parent molecule but is generated through its metabolic processing.

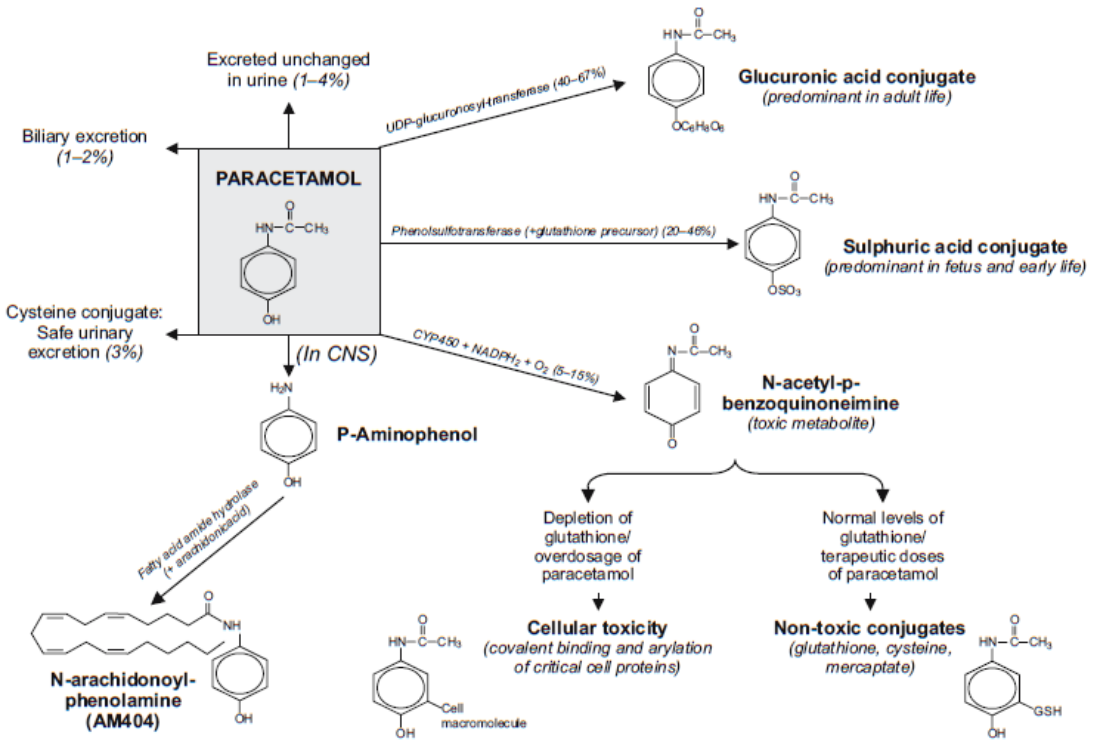

***Figure 10 Comprehensive metabolic pathways of APAP**. The diagram illustrates the primary Phase II detoxification routes, the CYP450-mediated bioactivation to NAPQI, and the FAAH-dependent conversion to the analgesic mediator AM404. [17,26,27]*

The liver processes APAP through two primary mechanisms: direct detoxification and metabolic bioactivation [26]. Under therapeutic conditions, approximately 85-90% of the dose is metabolized through phase II conjugation reactions, producing hydrophilic, non-toxic metabolites that are readily excreted via the renal route [27]. The renal clearance of unmetabolized APAP is minimal, with less than 5% of the administered dose being recovered unchanged [26,27]. However, a small but significant fraction of the drug escapes these primary pathways, undergoing an oxidative process that generates a highly reactive intermediate, which is responsible for the drug's potential hepatotoxicity.

Phase II Conjugation: Glucuronidation and Sulfation

Unlike many other xenobiotics, APAP does not strictly require Phase I functionalization for its elimination, as its phenolic hydroxyl group allows for direct Phase II conjugation and this is a key factor in its pharmacological safety at therapeutic doses [17,26]. The two primary pathways for APAP elimination are glucuronidation and sulfation [26].

- Glucuronidation: this represents the quantitatively dominant pathway (especially in adults [25]). It is mediated by UDP-glucuronosyltransferase enzymes, primarily

UGT1A1 and UGT1A6 [27]. APAP-glucuronide (APAP-gluc) is the most abundant metabolite, accounting for approximately 52-57% of the total metabolites recovered in urine [27].

- Sulfation: this reaction is catalyzed by sulfotransferases, mainly SULT1A1, producing APAP-sulfate. This conjugate constitutes about 30-44% of the administered dose [27].

A critical pharmacokinetic distinction between these routes is their respective capacity and affinity. The sulfation pathway is characterized by high affinity but low capacity [26] and the limiting factor for sulfation is the availability of the inorganic sulfate donor, *3′-phosphoadenosine-5′-phosphosulfate* (PAPS) [25]. Consequently, a metabolic shift occurs, and glucuronidation - a lower-affinity but higher-capacity system- becomes the primary compensatory route for elimination [25–27]. However, once these primary detoxification pathways are overwhelmed, the metabolic disposition shifts toward toxic bioactivation [18].

The Central Deacetylation Pathway: p-aminophenol and AM404

As illustrated in the alternative pathway of **Figure 10**, a minor but pharmacologically significant portion of APAP follows an alternative route within the central nervous system. Through the action of the enzyme FAAH, APAP is converted into p-aminophenol, which then conjugates with arachidonic acid to form AM404 [17]. This specific bioactivation pathway is fundamental for the drug's analgesic effect, as it allows the molecule to interact with the endocannabinoid system and vanilloid receptors (TRPV1), bridging the gap between simple enzyme inhibition and central pain modulation [16,17].

Phase I Bioactivation and NAPQI Formation

The remaining fraction of the dose, approximately 10%, undergoes Phase I oxidative metabolism, primarily catalyzed by the cytochrome P450 system [27]. While several isoenzymes are involved, CYP2E1 is the principal catalyst for this reaction, with secondary contributions from CYP1A2 and CYP3A4 [26,27]. This pathway results in the formation of N-acetyl-p-benzoquinone imine (NAPQI), a highly reactive and electrophilic intermediate [17]. Under therapeutic conditions (less than 4 g/day), NAPQI is efficiently and rapidly scavenged by conjugation with the sulfhydryl group of reduced glutathione (GSH), a reaction that can occur spontaneously or be facilitated by glutathione S-transferases (GST).

This process yields non-toxic cysteine and mercapturic acid conjugates, which are subsequently eliminated via the renal route [27,28].

Mechanism of Hepatotoxicity: From GSH Depletion to Mitochondrial Damage

The transition from a safe pharmacological profile to hepatotoxicity occurs when the rate of NAPQI formation exceeds the liver's capacity to regenerate GSH. Once hepatic GSH reserves are depleted by approximately 70%, the reactive NAPQI is free to interact with cellular components [26]. The initiating event of toxicity is the covalent binding of NAPQI with the cysteinyl sulfhydryl groups of cellular proteins, resulting in the formation of APAP-protein adducts (APAP-AD) [26,28]. While adduct formation occurs throughout the cell, the binding to mitochondrial proteins is the definitive predictor of toxicity, as these adducts disrupt key enzymes involved in the electron transport chain and mitochondrial antioxidant defence [28].

Mitochondrial Oxidative Stress and Peroxynitrite Formation

The accumulation of mitochondrial protein adducts initiates a profound dysfunction in cellular respiration, primarily characterized by the impairment of the electron transport chain. The electron transport chain becomes damaged and starts to leak electrons, which leads to the overproduction of superoxide ($O_2^{\bullet -}$). This molecule then reacts with nitric oxide to form peroxynitrite ($ONOO^-$), a very aggressive oxidant. Peroxynitrite causes two main types of damage: it attacks mitochondrial proteins through a process called nitration and it damages mitochondrial DNA (mtDNA), compromise the organelle’s ability to function properly [26,28].

The Mitochondrial Permeability Transition and Necrosis

This severe oxidative stress eventually triggers the Mitochondrial Permeability Transition (MPT). When this happens, pores in the mitochondrial membrane open, causing the membrane potential to collapse. This is a terminal event for the cell because ATP synthesis stops completely. Furthermore, the mitochondria release proteins into the cytoplasm that move to the nucleus and cause DNA fragmentation [26,28]. The result of this energy collapse is oncotic cell death (necrosis). This type of damage is typically found in the centrilobular region of the liver. This specific area is the most affected because it has the highest concentration of CYP2E1 enzymes and the lowest natural levels of glutathione, making it highly vulnerable to NAPQI [25,28].

1.3.4 Structure-Activity Relationship (SAR)

The pharmacological profile of APAP is strictly dependent on its specific molecular architecture. The basic scaffold consists of a benzene ring substituted with two functional groups in the para (1,4) orientation: a phenolic hydroxyl group ($-OH$) and an acetamido group ($-NHCOCH_3$).

The Role of the Aromatic Ring and Para-Substitution

From a purely structural standpoint, the relative positioning of the substituents on the ring is the most critical factor for the drug's activity. The para orientation is essential to ensure the electronic stability and geometry required for the drug's efficacy. This specific 1,4 substitution is essential for the cytochrome P450 mediated bioactivation into the reactive intermediate NAPQI, which occurs primarily when the hydroxyl and amide groups are in the para position [27,28]. Furthermore, the para orientation is a fundamental geometric requirement for the drug's interaction with COX isoforms. APAP functions as a reducing agent that inhibits the peroxidase site of the enzyme [21]. The 1,4-relationship between the hydroxyl and acetamido groups provides the optimal electronic conjugation for this redox activity, allowing the molecule to effectively donate electrons and neutralize the radical intermediates necessary for COX activation [21].

The structural arrangement is equally essential for the indirect modulation of the endocannabinoid system. The analgesic effect of APAP in the central nervous system depends on its metabolic conversion into AM404 [17]. This process requires the initial deacetylation of the molecule to form p-aminophenol. The specific para substitution of this intermediate is strictly necessary for its subsequent conjugation with arachidonic acid; any shift to ortho or meta position would result in structural analogues incapable of being recognized by the FAAH enzyme or effectively binding to cannabinoid receptors and vanilloid channels [16,17]. Consequently, the 1,4-configuration represents the critical chemical key that allows APAP to bridge the gap between peripheral COX inhibition and central antinociceptive pathway.

The Role of the Acetamido Group

The Acetamido Group at the para position represents the second functional pillar of APAP's structure. This specific N-acyl chain is responsible for the molecule's balance between lipid solubility and metabolic stability. The two carbon length of this N-acyl chain is optimal for the molecule's recognition by Phase II enzymes, such as UGT and SULT, which facilitate the primary detoxification pathway [26,27]. However, this group is also the specific site for the formation of the toxic quinone imine system. The nitrogen-carbon bond and the carbonyl group allow for the electronic stabilization of the transition state during cytochrome mediated oxidation, primarily involving CYP2E1 [28]. Modifications to these nitrogen substituents significantly alter the rate of bioactivation and, consequently, the drug's hepatotoxic potential [25,26,28]. In summary, the precise para arrangement of these functional groups creates a unique chemical entity capable of bridging peripheral COX inhibition and central antinociceptive pathways, while simultaneously defining its narrow therapeutic window [16,17,28].

1.4 Case Study: Acetaminophen and Clinical Monitoring

The need for high-efficiency capillary columns in this context is not merely a technical exercise but a clinical necessity. As detailed in the following sections, the limitations of current diagnostic tools and the extreme polarity of APAP's primary metabolites require the superior resolution and sensitivity provided by optimized micro-scale chromatographic systems [5,6].

1.4.1 The Gold Standard: The Rumack-Matthew Nomogram

Historically, the assessment of liver damage risk following acute APAP overdose has been based on the Rumack – Matthew nomogram (**Errore. L'origine riferimento non è stata trovata.**). This clinical tool, developed in the 1970s, relates the plasma concentration of APAP to the time elapsed since ingestion to predict the likelihood of hepatic necrosis and determine the necessity of N-acetylcysteine (NAC) administration [29]

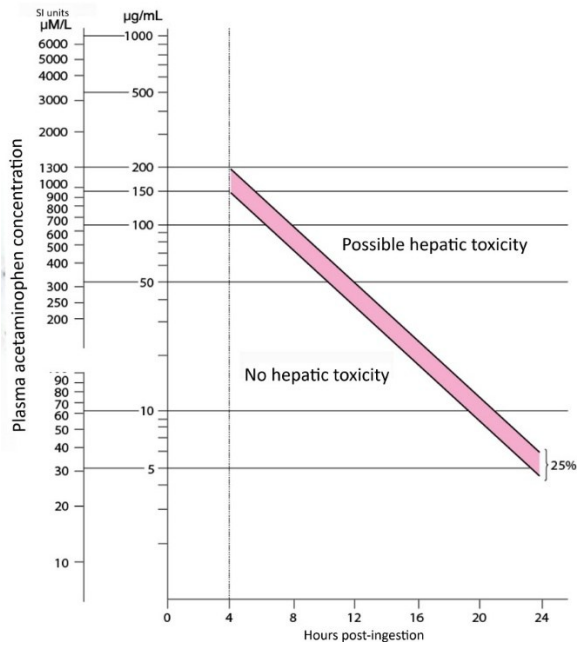

Figure 11: Rumack-Matthew nomogram for predicting acetaminophen-induced hepatotoxicity. *The solid red line indicates the threshold for probable hepatic damage, incorporating a 25% safety margin to account for variables in ingestion timing. Adapted from [29]*

Despite its undeniable success in emergency medicine, this model presents significant clinical limitations that necessitate a more comprehensive analytical approach [25]. A primary constraint is its temporal dependency, as the nomogram requires precise knowledge of the exact time of ingestion, a detail that is frequently unavailable or unreliable in cases of intentional overdose [25]. Furthermore, the model is inadequate for assessing chronic exposure, such as repeated supratherapeutic ingestions, where severe liver damage can manifest even when plasma concentration remain below the conventional treatment line [25]. Perhaps most critically, the nomogram focuses exclusively on the parent drug, thereby ignoring individual metabolic variability and the induction of enzymes like CYP2E1 [26,27].

1.4.2 Advanced strategies for comprehensive metabolic profiling

To overcome the inherent limitations of conventional prognostic tools, modern toxicological research has shifted toward comprehensive metabolic profiling. Instead of monitoring the parent drug alone, current strategies emphasize the simultaneous quantification of APAP and its full metabolic suite, including glucuronide and sulfate conjugates, as well as oxidative derivatives linked to the NAPQI pathway [26,27]. This approach allows for a more accurate assessment of an individual's real – time detoxification capacity and specific

toxicological risk, particularly when enzymatic induction or glutathione depletion is suspected [27,28].

However, the simultaneous determination of these compounds presents significant analytical challenges. The broad range of chemical polarities, spanning from the parent drug to highly hydrophilic conjugates, requires high-efficiency chromatographic systems capable of maintaining resolution within complex biological matrices [26,30]. A pivotal advancement in addressing these challenges is the development of tailor-made capillary microcolumns with optimized stationary phases, designed to enhance the retentivity of polar analytes while maintaining high mass transfer efficiency [4,8]

Specifically, this methodology focuses on the rational synthesis and screening of diverse polymeric compositions to evaluate how the stationary phase architecture influences the retention behavior of each APAP metabolite [30]. By synthesizing and testing columns with diverse polymeric compositions, it is possible to manipulate the selectivity of the system to suit these specific analytical needs. The application of mathematical retention models allows for the precise calculation of retention parameters, providing a fundamental framework for evaluating each specific polymer. This systematic approach facilitates the simulation of optimal gradient profiles, aiming to ensure the maximum resolution between critical pairs, such as APAP-glucuronide and APAP-sulfate, while minimizing the total analysis time [30]. By transitioning from empirical trial-and-error to mathematical retention prediction, it is possible to enhance the resolution of even minor oxidative metabolites from the biological background, bridging the gap between theoretical analytical chemistry and practical diagnostic needs [30].

Ultimately, the integration of predictive modelling into HPLC method development provides a robust and versatile platform for drug monitoring. This systematic approach ensures that high analytical standards are met even when dealing with the inherent variability of biological samples, effectively laying the groundwork for targeted applications in advanced clinical and forensic diagnostics [30].

1.4.3 Innovative Sampling and Matrix Analysis

The evolution of APAP monitoring is also closely linked to the development of innovative sampling techniques that aim to simplify clinical protocols and increase analyte stability. Among these, Volumetric Absorptive Microsampling (VAMS) has gained significant attention as a minimally invasive alternative to traditional venous blood collection. This

technique allows for the precise collection of fixed, small volumes of blood, which are then dried and analyzed via LC-MS/MS to quantify both the parent drug and its primary metabolites [31]. The use of VAMS not only improves patient compliance but also ensure high sample stability at room temperature, facilitating large-scale toxicokinetic studies.

In addition to blood-based microsampling, the analysis of urinary profiles remains a cornerstone for understanding the complete metabolic fate of APAP. Urinary matrices provide a non-invasive window into the total excretion of glucuronide and sulfate conjugates, as well as the identification of mercapturic acid derivatives, which are crucial indicators of the NAPQI detoxification pathway [32].

However, the transition toward these complex and miniaturized samples, such as dried blood or urine, requires analytical tools with superior sensitivity and miniaturization. In this perspective, the development of capillary microcolumns and the optimization of micro-scale chromatographic separations represent the necessary technological response to the demands of modern clinical and forensic toxicology (**Figure 12**) [31,32].

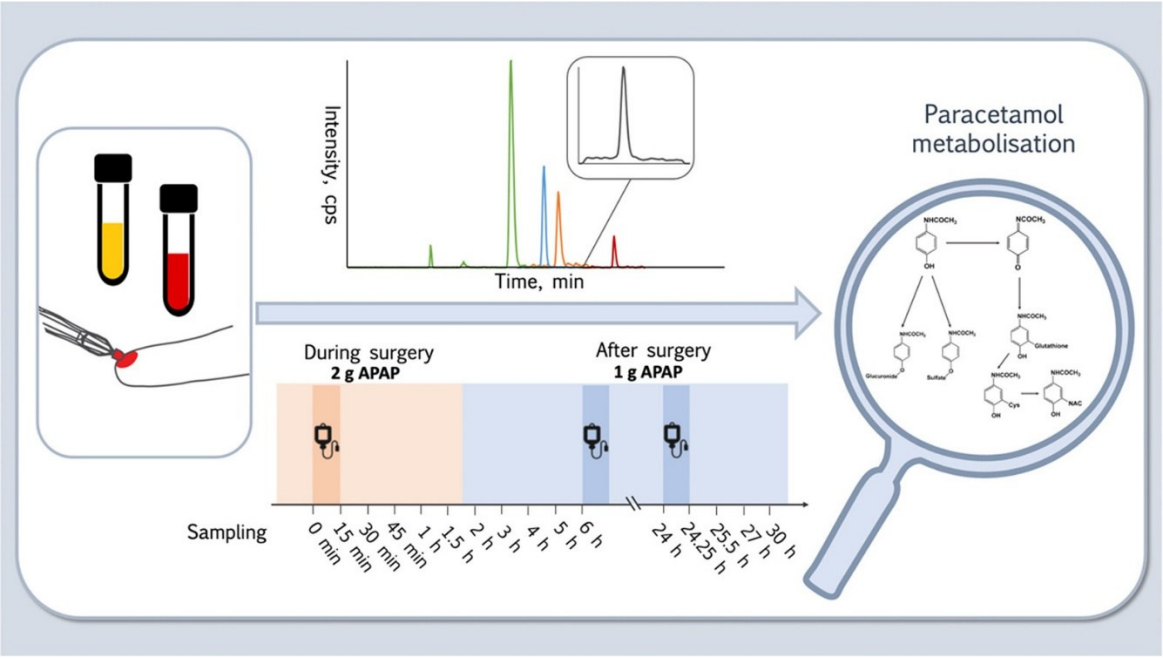

Figure 12: Integrated analytical workflow for APAP metabolic monitoring. *The scheme illustrates the clinical sampling timeline by Volumetric Absorptive Microsampling (VAMS) following intravenous administration, the representative HPLC-MS/MS separation of the metabolites The biochemical pathways link the detected analytes to the hepatic detoxification routes. Source from Delahaye et al. [31].*

2. Aim of the study

The present experimental research, conducted at the University of Pardubice, focuses on the development and chromatography characterization of innovative (poly)methacrylate-based monolithic stationary phases for microcolumn liquid chromatography.

The primary objective of this study was to conduct a comprehensive screening of various cross-linking agents influence the final separation efficiency. and kinetic performance [9,15]. This systematic approach aimed to build a robust technological foundation for the engineering of "tailor-made" columns for small molecule separations [33]

Drawing from the foundational studies on cross-linker effects [9,15], the experimental activity involved a systematic synthesis of nine different monolithic stationary phases. The research explored various classes of cross-linking agents, including:

- Ethylene glycol-based dimethacrylates, such as Ethylene glycol dimethacrylate (EDMA), Triethylene glycol dimethacrylate (TriEDMA), and Tetraethylene glycol dimethacrylate (TeEDMA), used to evaluate the influence of an increasing length of the hydrophilic ethylene glycol chain on the monolithic structure.
- Aliphatic dimethacrylates with different alkyl spacer lengths, including 1,3-butanediol dimethacrylate (1,3-BUDMA), 1,4-butanediol dimethacrylate (1,4-BUDMA), hexamethylene dimethacrylate (HEDMA), and decane-1,10-diol dimethacrylate (DeEDMA), to investigate the impact of increasing hydrophobicity, due to increasing spacer length, on the separation of small molecules.
- Aromatic dimethacrylates, specifically PhDMA (1,4-phenylene dimethacrylate), to explore the effect of a rigid aromatic core within the polymeric network.
- Multifunctional acrylates, such as PETRA (pentaerythritol triacrylate), which served as a benchmark to assess the impact of a high cross-linking density.

The detailed chemical structures, abbreviations, and specific structural features of the nine cross-linking agents evaluated are summarized in **Table 1**.

Table 1: Overview of the cross-linking library organized by structural trends.

Name & Abbreviation	Chemical Structure	Structural Features
Ethylene glycol dimethacrylate (EDMA)	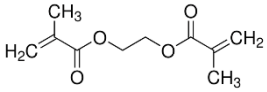	Baseline hydrophilicity; shortest oxyethylene chain.
Triethylene glycol dimethacrylate (TriEDMA)	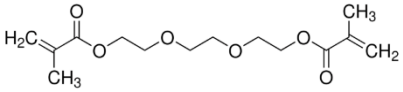	Increased hydrophilicity; 3 oxyethylene units.
Tetraethylene glycol dimethacrylate (TeEDMA)	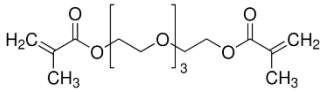	Maximum hydrophilicity; 4 oxyethylene units.
1,3-Butanediol dimethacrylate (1,3-BUDMA)	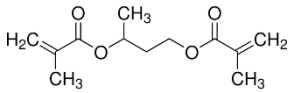	Short aliphatic spacer; branched isomer.
1,4-Butanediol dimethacrylate (1,4-BUDMA)	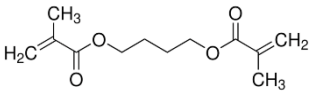	Linear aliphatic spacer; 4-carbon chain.
1,6-Hexanediol dimethacrylate (HEDMA)	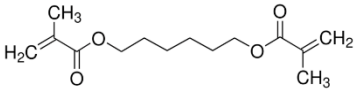	Moderate lipophilicity; 6-carbon alkyl spacer.
1,10-Decanediol dimethacrylate (DeEDMA)	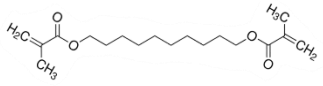	High lipophilicity; long 10-carbon alkyl spacer.
1,4-Phenylene dimethacrylate (PhDMA)	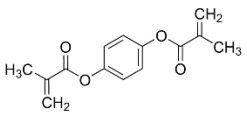	Structural rigidity; aromatic core for $\pi - \pi$ interactions.
Pentaerythritol triacrylate (PETRA)	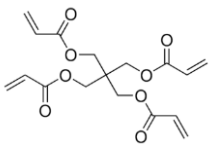	High cross-linking density; trifunctional acrylate benchmark.

The experimental workflow was developed through the following key steps:

- Surface Activation: A rigorous multi-step functionalization of the fused-silica capillary walls to ensure the covalent attachment and mechanical stability of the polymer bed.
- In-situ Synthesis: The preparation of monolithic phases by precisely controlling the polymerization mixture, using Lauryl methacrylate as the functional monomer and thermal initiation.
- Chromatographic Evaluation: The systematic testing of the synthesized columns using a homologous series of alkylbenzenes to determine the Height Equivalent to a Theoretical Plate (HETP) and permeability.

Ultimately, this comprehensive screening of cross-linkers aims to provide a robust technological foundation for the development of high-efficiency miniaturized tools. To validate the practical utility of the synthesized library, the most promising phases, specifically TeEDMA, TriEDMA, and 1,4-BUDMA, were selected for the optimization of a micro-HPLC method for acetaminophen (APAP) and its metabolic profile, supporting advanced retention models [12] for drug monitoring in complex biological matrices.

3. Materials and Methods

3.1 Chemicals and Reagents

All chemicals used in this study were of analytical grade and were used as received, without further purification. The monomers, cross-linkers, and initiators used for the synthesis of the monolithic stationary phases, along with the reagents for surface activation and chromatographic testing, are summarized in **Table 2**.

Table 2 List of chemicals used in the study, including their IUPAC names, purity, and suppliers.

Chemical Name (IUPAC)	Purity	Role	Supplier
Lauryl methacrylate (LMA)	96%	Functional monomer	Merck Life Science (Prague, CZ)
2,2'-Azobis(2-methylpropionitrile) (AIBN)	98%	Thermal initiator	Merck Life Science (Prague, CZ)
1,4-diol Butanediol	99%	Porogenic solvent	Merck Life Science (Prague, CZ)
1-Propanol	≥ 99.5%	Porogenic solvent	Merck Life Science (Prague, CZ)
Pentaerythritol triacrylate (PETRA)	Technical Grade	Cross-linker	Sigma-Aldrich (St. Louis, MO, USA)
Ethylene glycol dimethacrylate (EDMA)	98%	Cross-linker	Merck Life Science (Prague, CZ)
Triethylene glycol dimethacrylate (TriEDMA)	95%	Cross-linker	Sigma-Aldrich (Steinheim, DE)
Tetraethylene glycol dimethacrylate (TeEDMA)	90%	Cross-linker	Sigma-Aldrich (Steinheim, DE)

Butane-1,3-diol dimethacrylate (1,3-BUDMA)	95%	Cross-linker	Sigma-Aldrich (Steinheim, DE)
Tetramethylene dimethacrylate (1,4-BUDMA)	95%	Cross-linker	Sigma-Aldrich (Steinheim, DE)
Hexamethylene dimethacrylate (HEDMA)	98%	Cross-linker	Sigma-Aldrich (Steinheim, DE)
Decane-1,10-diol dimethacrylate (DeEDMA)	98%	Cross-linker	Sigma-Aldrich (Steinheim, DE)
1,4-Phenylene dimethacrylate (PhDMA)	98%	Cross-linker	Sigma-Aldrich (Steinheim, DE)
3-(Trimethoxysilyl)propyl methacrylate	98%	Silanizing agent	Sigma-Aldrich (St. Louis, MO, USA)
Acetic acid (Glacial)	99.8%	pH adjustment	Merck Life Science (Prague, CZ)
Acetonitrile	HPLC grade	Mobile phase / Washing	Merck Life Science (Prague, CZ)
Sodium hydroxide (NaOH)	Analytical Grade	Etching Agent	Lach-Ner (Czech Republic)
Hydrochloric acid (HCl)	Analytical Grade	Surface protonation	Lach-Ner (Czech Republic)
Ethanol	≥ 99.8%	Washing solvents	Sigma-Aldrich (Steinheim, DE)

Ultrapure water (resistivity $18.2\ M\Omega \cdot cm$) was produced by a Milli-Q water purification system (Millipore, Bedford, MA, USA). Nitrogen (high purity, 99.99%) used for drying the capillaries was supplied by a local provider.

To evaluate the kinetic performance and the hydrophobic selectivity of the synthesized monolithic columns, a homologous series of alkylbenzenes was employed as a chromatographic test probes. This mixture allows for the determination of the methylene selectivity and the calculation of the Height Equivalent to a Theoretical Plate (HETP) under isocratic conditions. The compounds used for the preparation of the standard mixture are detailed in **Table 3**.

Table 3: Chemical properties and suppliers of the alkylbenzene homologous series used for column characterization.

Compound	Formula	Purity	Supplier
Benzene	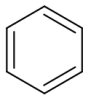	≥ 99.7%	Merck Life Science (Prague, CZ)
Toluene	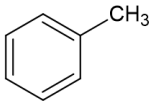	≥ 99.8%	Merck Life Science (Prague, CZ)
Ethylbenzene	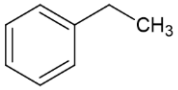	≥ 99%	Merck Life Science (Prague, CZ)
Propylbenzene	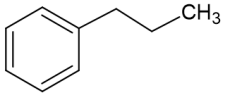	98%	Merck Life Science (Prague, CZ)
Butylbenzene	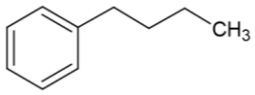	≥ 99%	Merck Life Science (Prague, CZ)
Hexylbenzene	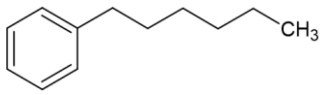	97%	Merck Life Science (Prague, CZ)
Octylbenzene	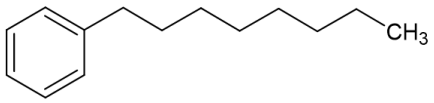	≥ 98%	Merck Life Science (Prague, CZ)

3.2 Equipment and Software

The experimental setup for the synthesis and characterization of the monolithic columns consisted of the following equipment:

Table 4**: **List of instruments and laboratory equipment.

Equipment	Model	Manufacturer
Micro-HPLC System	LC – 10 AD vp	Shimadzu (Japan)
UV-Vis Detector	Sapphire (External cell)	ECOM (Czech Republic)
Data Acquisition Software	Clarity (Version 8.x)	DataApex (Czech Republic)
Analytical Balance	Quintix	Sartorius (Germany)
Ultrasonic Bath	Fisherbrand™ FB15052	Fisher Scientific (MA, USA)
Thermostatic Oven	FN 400	Nüve (Ankara, Turkey)
Microscope	Optical Microscope	Fisher Scientific (Waltham, MA, USA)
Fused-Silica Capillaries	320 µm and 500 µm I.D.	Polymicro Technologies (USA)
Syringe Pump	NE-1000 (Single Syringe Pump)	New Era Pump Systems, Inc. (USA)
Scanning Electron Microscopy (SEM)	VEGA3	Tescan, Brno, Czech Republic

The chromatographic data acquired via Clarity software were further processed and visualized using the following tools:

- Microsoft Excel: Used for the preliminary organization of raw data, calculation of retention factors (k), and basic statistical parameters.
- Python (Matplotlib/Seaborn libraries): Employed exclusively for high-quality graphical representation, including the generation of Van Deemter plots (HETP vs. linear velocity) and Martin plots (log k vs. carbon number). This approach ensured superior graphical resolution and customized formatting for the final thesis.

3.3 Capillary Surface Modification

The inner surface of the fused-silica capillaries was chemically modified to ensure the stability and covalent attachment of the monolithic bed. For each batch, a 1-meter long fused-silica capillary was used to ensure uniform treatment across all subsequent segments. The activation and silanization procedure were carried out following the protocol described by P. Jandera et al. [9].

3.3.1 Surface Activation (Etching)

Before the synthesis of the monolithic bed, the 1-meter capillary underwent a fundamental activation process to increase the density of reactive sites. Initially, the capillary was continuously flushed for 30 minutes with acetone, followed by 30 minutes with distilled water.

Subsequently, it was subjected to an alkaline etching step by flushing a 1.0 M sodium hydroxide (NaOH) solution for 30 minutes. During this stage, the hydroxide ions promote the hydrolysis of the siloxane bridges (Si–O–Si), leading to the formation of deprotonated surface silanol groups ($Si - O^-$), as previously illustrated and explained in Chapter 1.1.2 (page 11). After this, the system was rinsed again with distilled water for 30 minutes until the effluent reached neutrality, followed by a 30-minute wash with 0.1 M hydrochloric acid (HCl). This acidic treatment is crucial to ensure the complete protonation of the surface, converting the ($Si - O^-$) sites into active silanol groups (Si–OH). A final rinsing cycle with ethanol (EtOH) for 30 minutes was performed to eliminate any residual inorganic species.

3.3.2 Surface Silanization

The second phase of the capillary treatment involved the covalent functionalization of the activated silanol groups to create a stable anchoring layer for the monolithic scaffold. A silanizing solution was prepared by dissolving 20% (v/v) 3-(trimethoxysilyl) propyl methacrylate in ethanol. The reaction mechanism involves the hydrolysis of the methoxy groups of the silanizing agent, followed by their condensation with the surface silanols. This creates a stable covalent "bridge" that terminates with a reactive methacrylate moiety, which will later participate in the radical polymerization of the monolith.

The experimental procedure was performed by continuously flushing the capillary with this silanizing mixture for 3 hours at room temperature. This constant flow ensured a uniform reaction and the establishment of a stable bridge between the inorganic silica wall and the

organic methacrylate functionalities. Upon completion of the reaction, the capillary was rinsed with ethanol for 30 minutes to remove any unreacted silanizing agent, followed by thorough drying under a stream of nitrogen. Finally, the entire 2-meter capillary was left to equilibrate at room temperature for 24 hour before any further manipulation. This stabilization period is essential to ensure the complete formation and long-term stability of the covalent bonds, preventing any displacement or extrusion of the monolithic bed during high-pressure chromatographic runs.

3.4 Synthesis of Monolithic Columns

Following the 24-hours stabilization period, the pre-activated 2-meter capillary was cut into shorter segments to prepare approximately four individual columns (ca. 25 cm each). For each synthesis, the polymerization mixture was formulated by accurately weighing the components into a glass vial. The monomeric phase consisted of 20% (w/w) of lauryl methacrylate (LMA) as the functional monomer, which was mixed with a specific cross-linking agent (15% w/w). A central objective of this research was the systematic comparison of various cross-linkers to evaluate their impact on the final monolithic structure and chromatographic performance. The study included a broad range of cross-linking agents, specifically:

- Ethylene glycol-based dimethacrylates: EDMA, TriEDMA, TeEDMA.
- Aliphatic dimethacrylates: 1,3-BUDMA, 1,4-BUDMA, HEDMA, DeEDMA.
- Multifunctional and rigid agents: PETRA and 1,4-phenylene dimethacrylate (PhDMA).

To this monomeric mixture, the thermal initiator 2,2'-azobis(2-methylpropionitrile) AIBN (1% w/w) and a porogenic solvent system consisting of 1,4-butanediol (24% w/w) and 1-propanol (40% w/w) were added. The vial was then agitated until a completely clear and homogeneous solution was obtained, ensuring the total dissolution of the initiator.

Each capillary segment was manually filled with the polymerization mixture using a micro-syringe, maintaining a steady flow to prevent the formation of air bubbles. Once filled, the ends were securely sealed with silicone rubber stoppers, and the capillaries were placed in a thermostatic oven at 60 °C for 20 hours. This thermal treatment triggered the radical polymerization and subsequent phase separation. Finally, each completed column was rinsed for one hour with acetonitrile using a manual pressure pump to remove the porogenic

solvents and any residual unreacted monomers, leaving the monolithic bed ready for characterization.

3.5 Chromatographic Characterization

The synthesized monolithic columns were evaluated through a systematic chromatographic study to determine their performances in term of efficiency, selectivity and stability. The primary goal of this characterization was to assess the quality of the monolithic bed and to optimize the separation conditions by identifying the kinetic parameters that govern the chromatographic process.

3.5.1 Experimental Configuration and Conditions

The chromatographic analyses were performed using the micro-HPLC setup described in **Figure 13**. To ensure high-quality data and minimize extra-column band broadening, which is a critical factor in capillary chromatography, the detection window was prepared on a separate segment of fused-silica capillary immediately after the monolithic bed. This detection segment was connected to the monolithic column using a low-dead-volume micro-connector. The detection window was created by carefully burning off a small section (approximately 1–2 mm) of the polyimide coating using a controlled flame. After the thermal removal, the charred residues were cleaned with ethanol to ensure a perfectly transparent optical path. This post-column detection configuration allowed the UV-Vis detector to monitor the analytes as they emerged from the monolith and passed through the connection interface. Great care was taken during the assembly to ensure a perfectly squared abutment between the two capillary ends within the connector, thereby minimizing potential sources of dead volume and peak dispersion that could arise at the junction.

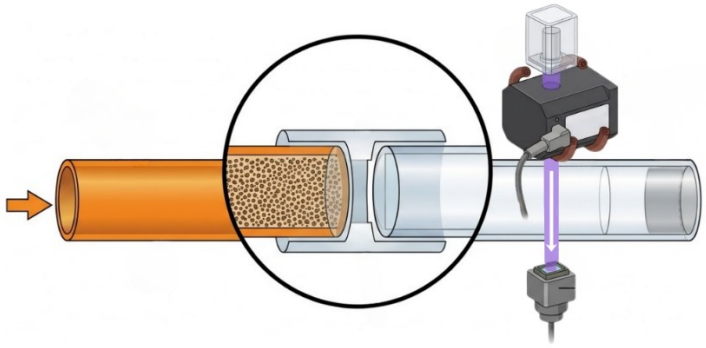

Figure 13: Schematic representation of the post-column detection configuration. *The monolithic capillary column is connected to a transparent detection segment via a low-dead-volume micro-union. The detection window was prepared by thermal removal of the polyimide coating to allow UV-Vis monitoring. Created with Canva.*

All characterization tests were conducted under isocratic conditions to allow for an accurate calculation of the retention factor (k) and column efficiency. The mobile phase was mainly composed of a mixture of acetonitrile and water in an 80:20 (v/v) ratio. This ratio was consistently used for most of the chromatographic runs to ensure sufficient elution power for the hydrophobic test analytes. The mobile phase was degassed via ultrasonication prior to use and also on-line to prevent the formation of air bubbles that could interfere with the signal in the micro-capillary detection system. The test mixture included a homologous series of alkylbenzenes, specifically benzene, toluene, ethylbenzene, propylbenzene, butylbenzene, hexylbenzene, and octylbenzene, to evaluate the hydrophobic selectivity and the overall efficiency of the methacrylate-based monolithic stationary phases. To study the kinetic performance and the effect of mobile phase velocity (u) on peak variance (σ^2), the flow rate was systematically varied, typically ranging from 1 to 50 µL/min.

3.5.2 Morphological Characterization (SEM)

To correlate the chromatographic performance with the internal physical structure of the monoliths, a morphological investigation was conducted using Scanning Electron Microscopy (SEM). This analysis provided direct visual evidence of the polymer globule size, pore interconnectivity, and the quality of the attachment to the capillary wall.

The samples were prepared and analyzed according to the following protocol:

- Sample Preparation: Small segments (ca. 2–3 mm) were carefully cut from each monolithic column using a high-precision ceramic capillary cutter to ensure a clean and perpendicular cross-section.

- Sputter Coating: To ensure electrical conductivity and prevent surface charging during imaging, a common issue with organic polymers, the samples were mounted on aluminum stubs and coated with a thin layer of gold.
- Observation: The internal structure, globule size, and wall adhesion were then observed using the VEGA3 Tescan microscope (Brno, Czech Republic) at an accelerating voltage of 15 kV. Micrographs were acquired at different magnifications to evaluate the monolith at different scales:
    - 400x: to assess the overall radial homogeneity and the adherence of the polymer to the fused-silica wall.
    - 900x: to observe the distribution of the interconnected flow-through macropores.
    - 4000x: to investigate the fine morphology and size of the individual polymer microglobules.

3.5.3 Data processing and Efficiency Parameters

The chromatographic data were processed using Clarity software (DataApex, Czech Republic) to extract retention times (t_R) and peak widths at half height ($w_{0.5}$). To normalize the retention behaviour and decouple it from the column dimensions and flow rate, the retention factor (k) was calculated for each analyte as follows:

$$k = \frac{t_R - t_0}{t_0}$$

In this study, t_0 (column void time) was determined theoretically, based on the geometric volume of the capillary and the total porosity of the monolithic bed. Conversely, t_R was obtained experimentally from the chromatograms, representing the elution time of the individual peaks for each analyte in the homologous series. This approach allows for a precise evaluation of the thermodynamic interactions between the analytes and the stationary phase, independent of experimental fluctuations in the solvent front.

The linearity of the retention mechanism was assessed by plotting the logarithm of the retention factor ($\log k$) against the number of carbon atoms (n) in the homologous series of alkylbenzenes, according to the Martin equation:

$$\log k = A \cdot n + B$$

In this linear relationship, the slope (A) represents the methylene group selectivity, which indicates the ability of the stationary phase to differentiate between successive members of the homologous series, while the intercept (B) is a constant related to the interaction of the phenyl group with the matrix. The quality of the fit for each stationary phase was statistically evaluated using the coefficient of determination (R^2), obtained through linear regression analysis.

To evaluate the separation quality of the synthesized monoliths, the number of theoretical plates (N) was calculated for each analyte using the following equation:

$$N = 5.54 \cdot \left(\frac{t_R}{w_{0.5}}\right)^2$$

The columns efficiency was further characterized by the height equivalent to a theoretical plate (H), defined as:

$$H = \frac{L}{N}$$

where L is the effective length of the monolithic bed. The kinetic performance was analyzed by monitoring the linear velocity (u) of the analytes, calculated as follows:

$$u = \frac{L}{t_r \cdot 60}$$

The factor of 60 was applied to convert the retention time from minutes to seconds, expressing velocity in mm/s. The study of band broadening was centered on the peak standard deviation (σ) in the time domain, derived from the experimental data as:

$$\sigma = \frac{t_R}{\sqrt{N}}$$

To identify the best operating conditions for the micro-HPLC system, peak dispersion was volumetrically optimized by evaluating the product of the standard deviation and the mobile phase flow rate (F):

$$\sigma_v = F \cdot \sigma_t$$

This parameter, expressed in microliters (µL), allowed for a direct assessment of the volumetric dispersion. Estimating peak width in volumetric terms is more appropriate because band broadening occurs as a spatial dispersion inside the column; while time-based width changes with flow conditions, the volumetric width provides a more fundamental measure of the column's performance.

3.6 Preparation of Acetaminophen and its Metabolites for HPLC Analysis

Chromatographic efficiency and selectivity of the synthesized monolithic columns were evaluated by analyzing analytical standards of APAP and its main polar metabolites: acetaminophen-cysteine (ACYS), acetaminophen-N-acetylcysteine (ANAC), and acetaminophen-glutathione (ASG). These compounds were obtained and characterized according to the synthetic procedures detailed by Vanova et al. [30]

Individual stock solutions were prepared by dissolving the pure compounds in ultra-pure distilled water (Milli-Q grade) to reach a target concentration of approximately 10 mg/L. This concentration was selected to ensure an optimal analytical signal for the subsequent characterization. To ensure complete dissolution and homogeneity of the samples, the solutions were subjected to magnetic stirring and brief ultrasonication. All chromatograms were recorded at a detection wavelength of 445 nm, which was selected to optimize the monitoring of the target analytes based on their spectrophotometric properties.

4. Results and Discussion

4.1 Global Assessment of Chromatographic Performance

This chapter evaluates the results obtained from the synthesis and characterization of various capillary monolithic columns. The investigation focuses on the influence of different cross-linkers and functional monomers on the support morphology and the resulting kinetic performance.

To provide a comprehensive overview, **Table 5** summarizes the fundamental chromatographic and kinetic parameters ($t_r, w_{0.5}, k, N, H$) for each synthesized column, calculated using a homologous series of alkylbenzenes under isocratic conditions. In accordance with established literature [30], benzene was identified as the first eluted peak of the series. Consequently, benzene was selected as the reference probe for the calculation of the column efficiency.

***Table 5**: Summary of chromatographic and kinetic parameters*

Cross-linkers	ID (µm)	L (mm)	t_0 (min)	t_r (min)	$w_{0,5}$	k	N	H_{min} (µm)	P (MPa)	F (µL/min)
EDMA	320	180	3.47	7.22	0.29	0.25	3437.00	52.37	1	2
TriEDMA	320	229	7.37	17.43	0.60	1.38	4677.83	48.95	1	2
TeEDMA	320	105	3.38	7.00	0.34	1.13	2352.40	44.64	1	2
1,3 BUDMA	320	128	4.12	6.98	0.54	1.13	925.66	138.28	1	2
1,4 BUDMA	320	220	7.08	29.48	0.64	1.68	11762.70	18.70	0.2	2
HEDMA	320	192	6.18	12.38	0.42	1.00	4815.42	39.87	2	2
DeEDMA	320	124	3.99	7.50	0.50	1.15	1587.46	78.11	1	2
PhEDMA	320	130	n.d.	24.80	n.d	n.d	n.d	n.d.	1	2
PETRA	320	107	3.44	3.92	0.30	0.14	945.29	113.19	1	2

The experimental data reported in **Table 5** reveal a diverse range of behaviors across the different polymeric matrices. While the ethylene glycol-based series shows a general trend of increasing efficiency with increasing spacer length, other phases present unique characterization profiles. Specifically, the PhEDMA column exhibited such severe band broadening and unstable retention behavior that the extraction of reliable quantitative parameters was not feasible. On the other hand, the 1,4 BUDMA phase yielded exceptionally high calculated efficiency results, showing the lowest plate height ($H_{min} = 18,70\ \mu m$) of the entire set. However, as will be discussed in the following sections, these mathematical results for the 1,4 BUDMA phase do not fully translate into reliable chromatographic performance. This apparent efficiency is likely influenced by non-ideal flow

distribution and the presence of large macropores, which may artificially narrow the measured peak width without reflecting true chromatographic performance. These preliminary observations serve as the foundation for the upcoming analysis of internal morphology, thermodynamic retention mechanisms, and kinetic modelling, which will critically evaluate and validate the performance gaps observed in this initial global assessment.

4.2 Morphological Characterization via SEM

The internal architecture of the nine synthesized monoliths was investigated via Scanning Electron Microscopy (SEM). The morphology of these materials is a direct result of the phase separation process, which is governed by the chemical nature, spacer length, and functionality of the cross-linkers [1,34].

4.2.1 The Ethylene Glycol Series (EDMA, TriEDMA, TeEDMA)

The first series of monoliths investigated explores the systematic effect of increasing the ethoxy-unit spacer length within the cross-linker molecule. The SEM micrographs reveal a clear and progressive morphological evolution across the series, transitioning from a clustered and poorly organized structure to a highly homogeneous and interconnected globular network (**Figure 14**). This evolution is critical for understanding the relationship between the chemical structure of the cross-linker and the resulting hydrodynamic properties of the stationary phase [1].

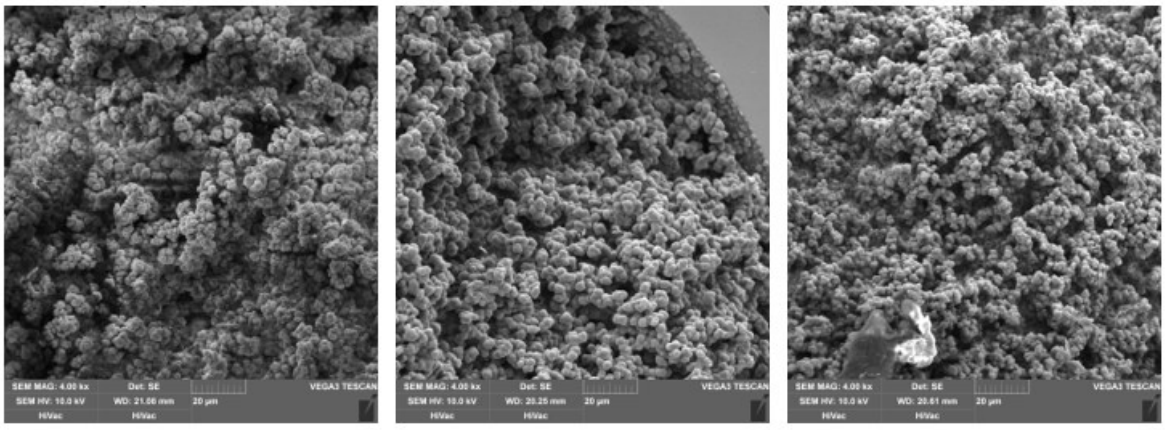

Figure 14: SEM micrographs of the ethylene glycol-based series. *(a) EDMA, (b) TriEDMA and (c) TeEDMA. The images (at 4000x magnification) show the progressive refinement of the globular structure and the improvement in pore interconnectivity as the cross-linker spacer length increases. Scale bar: 20 µm.*

The EDMA monolith, which utilizes the shortest spacer in this series, exhibits a standard globular structure but is characterized by relatively large aggregates and an uneven pore size distribution. Such a morphology often leads to non-ideal flow paths, which explains the lower chromatographic efficiency observed compared to its longer-chain counterparts. As the spacer length increases, moving to TriEDMA and finally to TeEDMA, a significant refinement of the internal architecture is observed: the polymer microglobules become smaller and more uniform and their interconnections with the flow-through pores becomes more regular [34].

The TeEDMA column exhibits the most optimized morphology of the entire study. The visual evidence of well-defined and consistent flow-through pore system correlates directly with the superior kinetic efficiency recorded during experimental testing. This relationship between pore homogeneity and chromatographic efficiency has been widely reported for methacrylate-based monoliths. The increased length and flexibility of the glycolic spacer in TeEDMA appear to stabilize the phase separation process during polymerization, preventing the premature formation of large, dense polymer clusters [9]. This observation is consistent with previous studies showing that increasing the flexibility of the cross-linker spacer can improve pore homogeneity and mass transfer properties in methacrylate monoliths [9,33].

As discussed in literature, achieving this balance between globular size and pore interconnectivity is essential for the separation of small molecules, such as paracetamol and its metabolites, where mass transfer resistance must be minimized [13,33]. The TeEDMA matrix provides a high surface to volume ratio while maintaining excellent permeability, fulfilling the requirements for high-performance liquid chromatography supports [2,35].

4.2.2 Aliphatic series (1,3-BUDMA, 1,4-BUDMA, HEDMA, DeEDMA)

The morphological investigation of the aliphatic series highlights how the use of pure alkyl spacers significantly affects the polymer architecture, leading to structures that are notably less optimized than the ethylene glycol-based counterparts [9]. While the glycolic monoliths represent the benchmark for homogeneity in this study, the aliphatic series exhibits a higher degree of structural irregularity. As illustrated in **Figure 15**, the 1,4 BUDMA (b) column stands out for its unique open cluster morphology. This structure is dominated by large polymer aggregates separated by oversized flow-through pores (macropores), providing a physical explanation for the permeability paradox encountered during testing: despite its

length, the columns generates extremely low backpressure because the mobile phase flows through these wide channels with minimal resistance [34].

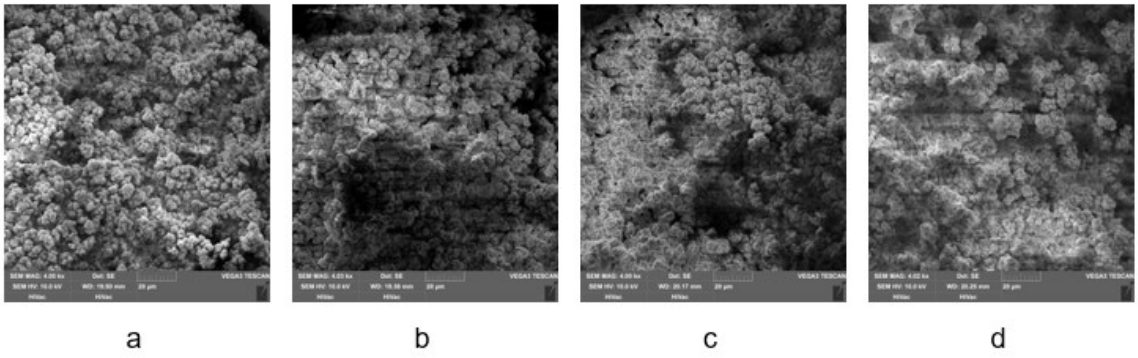

Figure 15: SEM micrographs comparing the aliphatic dimethacrylate series at 4000x magnification. *(a) 1,3-BUDMA, (b) 1,4-BUDMA, (c) HEDMA and (d) DeEDMA. The open structure of the 1,4-BUDMA matrix (b) is clearly visible, showing oversized macropores. Scale bar: 20 µm.*

Notably, while the 1,4-BUDMA column initially provided unexpectedly high plate count values during preliminary screenings, these SEM observations suggest a more complex reality. The presence of such large macropores indicates that the apparent efficiency was likely an artifact of the high permeability and non-ideal flow distribution, rather than a sign of a high-performing stationary phase [13]. This excessive openness is detrimental to stable chromatographic performance, as the wide channels reduce the effective surface area available for solute-stationary phase interactions, leading to kinetic instability and poor mass transfer [1,6].

Further analysis of the series shows that the 1,3-BUDMA (a) monolith develops a relatively more compact network compared to its linear isomer, likely due to different radical propagation rates during the polymerization process [1]. The HEDMA (c) column, featuring a longer C6 alkyl chain, presents a different trend, exhibiting distinct, spherical microglobules. While these structures are notably less heterogeneous and more uniform than the disordered aggregates seen in the 1,4-BUDMA matrix, the overall network still lacks the superior level of interconnectivity seen in the glycolic series [2]. Finally, in the DeEDMA (d) column, the high hydrophobicity of the C10 spacer appears to drive a less controlled phase separation, resulting in larger globular sizes and increased structural voids that complicate the separation of small molecules [35].

4.2.3 Poly-functional and Aromatic Matrices (PETRA, PhDMA)

The final morphological investigation focuses on monoliths synthesized with non-standard cross-linkers and monomers, which exhibit significant structural deviations from glycol series. As shown in **Figure 16**, these chemical variations resulted in catastrophic structural failures, ranging from incoherent porous networks to a total lack of capillary wall adhesion.

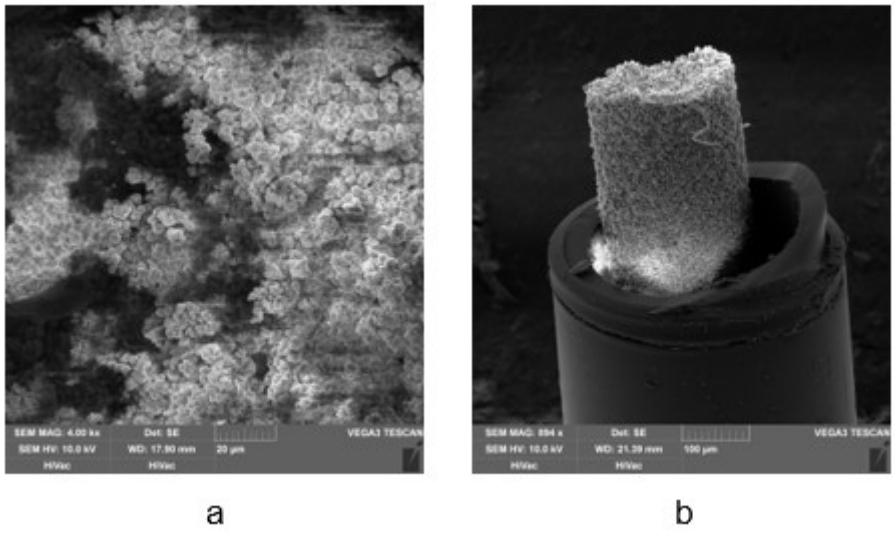

Figure 16: SEM micrographs of specialized monolithic matrices. *(a) PETRA: highly irregular and fractured network with visible hollows and structural excavations. (b) PhDMA: polymer rod fully detached from the fused-silica capillary wall. Magnification 4000x (a) and 894x (b). Scale bars: 20 µm and 100 µm.*

The PETRA (a) monolith, synthesized with a trifunctional acrylate cross-linker, presents a broken and extremely heterogeneous morphology. Instead of the expected dense network, the micrograph reveals a series of hollows and structural excavations, indicating that the high number of reactive sites led to an uncontrolled and premature phase separation. This lack of structural coherence prevents the formation of a stable globular bed, explaining the erratic hydrodynamic behavior and the poor performance observed during the screening phase [34].

Regarding the PhDMA (b), the primary morphological defect is the complete failure of the polymer to adhere to the capillary wall. As clearly visible in the low-magnification cross-section, the monolithic rod is entirely detached from the silica surface. This wall effect is a critical synthesis failure that allows the mobile phase to flow around the polymer rather than through it, rendering the column chromatographically inert [13]. Furthermore, the aromatic phenyl group of the PhDMA monomer appears to have hindered the formation of a uniform porous system, resulting in the disordered internal structure seen in the micrographs [6,35].

For these reasons, PhEDMA stationary phase was not considered for the separation of the test analytes

Overall, the SEM investigation highlights a clear relationship between the chemical structure of the cross-linker and the resulting monolithic architecture. Glycol-based cross-linkers promoted the formation of more homogeneous and interconnected globular networks, which translated into improved chromatographic performance. In contrast, purely aliphatic and multifunctional systems generated less controlled morphologies, leading to irregular pore structures and reduced chromatographic reliability.

4.3 Hydrodynamic and Thermodynamic Evaluation: Retention and Selectivity

In this section, the thermodynamic behavior of the synthesized monolithic columns is analyzed to determine the efficiency of the separation mechanism. The primary objective is to evaluate how the chemical architecture of the cross-linker affects the hydrophobicity and methylene selectivity of the stationary phase. Achieving a precise balance between surface chemistry and pore size distribution remains the fundamental challenge in optimizing organic monoliths for high-resolution small molecule separation [33].

4.3.1 Martin Plot Analysis

To investigate the interaction mechanism between the analytes and the polymer matrix, a homologous series of alkylbenzenes was utilized. Retention factors (k) were calculated based on a theoretical dead time (t_0), derived from the specific internal geometry of each capillary ($r = 0.0016\,mm$ and column length L) and a total porosity ($\varepsilon = 0.8$). The total porosity was assumed to be 0.8, a value representative for methacrylate based monoliths prepared with a high volume fraction of porogenic solvents, as described in the structural models proposed by Urban and Jandera [34]. The dead time was specifically calculated for each column using the formula $t_0 = \frac{V_0}{F}$, where V_0 ($V_0 = \pi \cdot r^2 \cdot L \cdot \varepsilon$) represents the internal volume of the capillary (dependent on its actual length) and F is the volumetric flow rate. This approach accounts for the slight variations in length and flow conditions among the different synthesized columns.

This assumption is consistent with the high permeability and low backpressure observed experimentally, confirming a highly porous interconnected network [9].

The Martin Plot represents the relationship between the logarithm of the retention factor ($\log k$) and the number of carbon atoms (n_c) in the alkyl chain. This method, based on the thermodynamic theory of partition chromatography, allows for the qualification of methylene selectivity ($\propto$) through the slope of the linear regression [36].

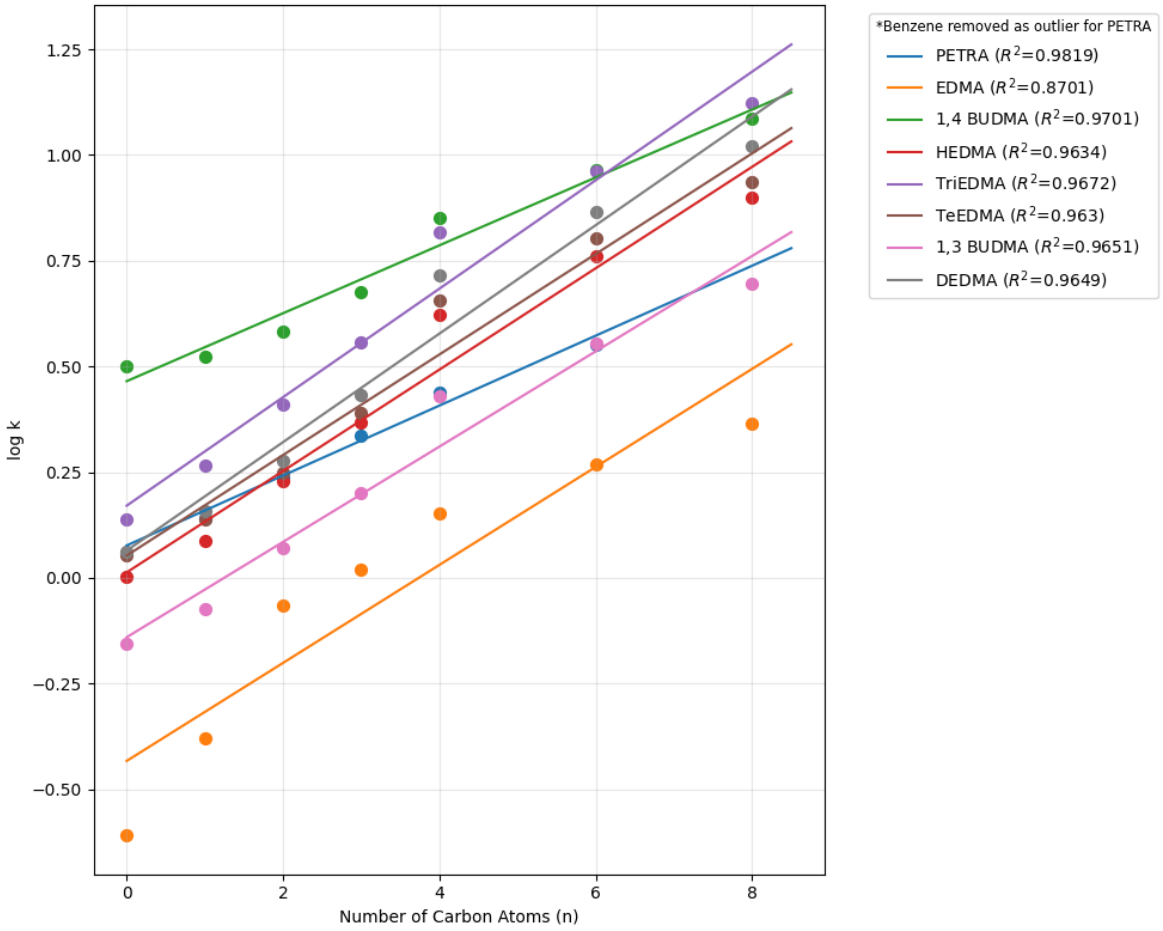

Figure 17:Comparative Martin Plot *($log\ k$ vs n_c) for the selected monolithic stationary phases. Experimental data were obtained at a flow rate of 2 μL/min. Note: For the PETRA column, benzene was treated as an outlier and excluded from the regression to yield an adjusted $R^2 = 0.9819$*

As shown in **Errore. L'origine riferimento non è stata trovata.** and detailed in **Table 6**, the thermodynamic consistency varies significantly across the different polymer matrices

Table 6: Linear regression parameters *($log\ k = \alpha \cdot n_c + \beta$) derived from the Martin Plots for the synthesized monolithic columns*

Stationary Phase	Slope (α)	Intercept (β)	Correlation (R^2)
EDMA	0.1159	-0.4329	0.8701
TriEDMA	0.1283	0.1707	0.9672
TeEDMA	0.1189	0.0527	0.963
1,3 BUDMA	0.1127	- 0.1404	0.9651
1,4 BUDMA	0.0803	0.4651	0.9701
HEDMA	0.1199	0.0129	0.9634
DeDMA	0.1283	0.0644	0.9649
PETRA	0.0827	0.0766	0.9819

The data summarized in **Table 6** highlights the direct correlation between the chemical structure of the cross-linker and the resulting chromatographic behavior. Achieving a precise balance between surface chemistry and pore size distribution remains the fundamental challenge in optimizing organic monoliths for high-resolution small molecule separation [33].

The column synthesized with TeEDMA, TriEDMA, DeEDMA, HEDMA and both BUDMA isomers demonstrate high thermodynamic consistency, with R^2 values exceeding 0.96. These high correlation coefficients are a direct indicator of a homogeneous stationary phase surface and uniform accessibility for the analytes [2]. The in-situ polymerization of monoliths, while simpler than traditional packing, must be optimized to avoid problems of homogeneity. In these columns, the high linearity confirms that the distribution of hydrophobic groups is energetically consistent, allowing for a predictable partition mechanism.

Whitin this group,1,4 BUDMA stands out for its high linearity ($R^2 = 0.9701$), although its significantly lower slope ($\alpha = 0.0803$) suggest that the presence of oversized macropores

reduces the effective surface area available for methylene interaction [14]. Conversely, the EDMA column, despite belonging to the glycol-based family, shows a lower correlation ($R^2 = 0.8701$), suggesting that the shorter spacer length may lead to a less organized or more rigid polymeric network that hinders ideal partition.

The most critical deviation is observed for the PETRA column ($R^2 = 0.6434$). The dramatic drop in linearity mathematically confirms the structural heterogeneity and tortuosity observed in the SEM micrographs. Such an inhomogeneous structure inescapably leads to a deterioration of column process [2]. This is a known limitation for highly branched cross-linkers in advanced LC application, where irregular flow paths prevent efficient small molecule separation [3].

4.3.2 Chromatographic Comparison at Low Flow

To further investigate the impact of polymer morphology on separation quality, a direct comparison of the chromatograms obtained at a low flow rate (2 µL/min) was performed. At this velocity, mass transfer resistance is minimized, allowing for a clearer evaluation of the intrinsic selectivity and column efficiency.

Before analyzing the separation for the homologous series, it is important to evaluate the overall profile of the chromatogram. The initial section reveals some minor signals and baseline fluctuations. These are likely attributable to the injection plug disturbance and the presence of trace impurities or residual monomer from the in situ polymerization process, a common occurrence in monolithic microcolumns that requires extensive washing cycles to be fully eliminated [2]. Despite these minor initial signals, the columns demonstrate excellent stability and performance for the target analytes.

Glycol-based Series: TeEDMA and TriEDMA

The columns synthesized with glycol-based cross-linkers exhibited the best chromatographic performance. The separation of the homologous series was carried out using a mobile phase composed of Acetonitrile/Water 80:20 (v/v) at a constant flow rate of 2 µL/min.

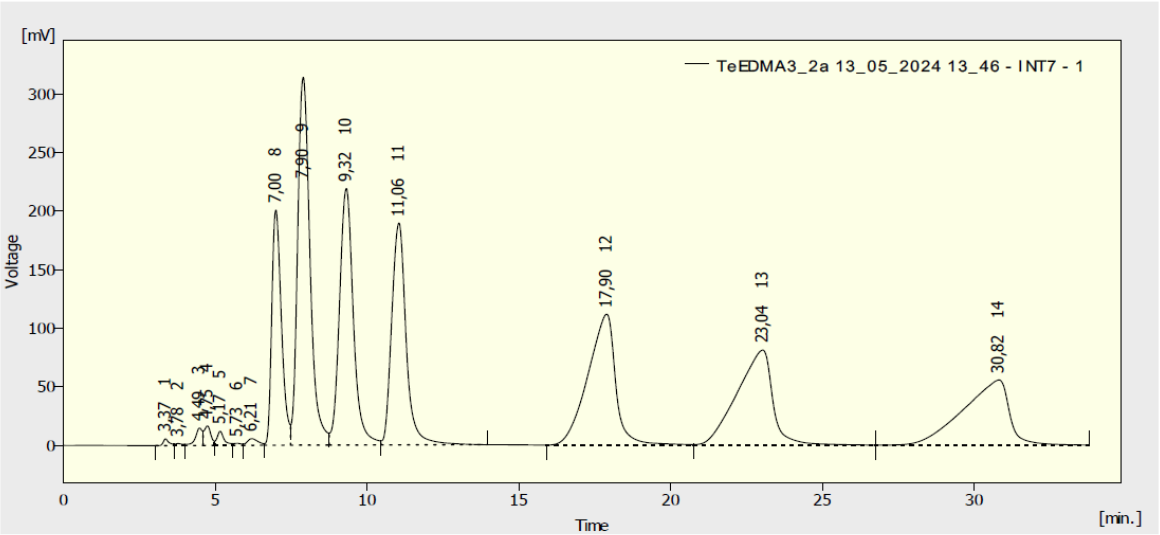

Figure 18: Chromatogram of alkylbenzenes separation on the TeEDMA monolithic column.

As shown in **Figure 18**, the TeEDMA column provides a high-resolution separation where all analytes (peaks 8 to 14) are well-resolved to the baseline. The peaks exhibit remarkable symmetry and narrow widths for the early-eluting compounds. This peak morphology is a clear indicator of an ideal partition mechanism and confirms the high energetic homogeneity of the stationary phase surface [2]. The stability of the successful baseline during the elution of the alkylbenzenes and the sharp peak profiles validate the successful formation of a uniform globular network, which minimizes dispersion phenomena and ensures efficient mass transfer [37]. These visual evidences are in full agreement with the high R^2 value (0.9630) obtained in the Martin Plot analysis.

Similar results were obtained for the TriEDMA column, which belongs to the same glycol-based family. The separation was performed under the same conditions (Acetonitrile/Water 80:20 v/v, 2 µL/min).

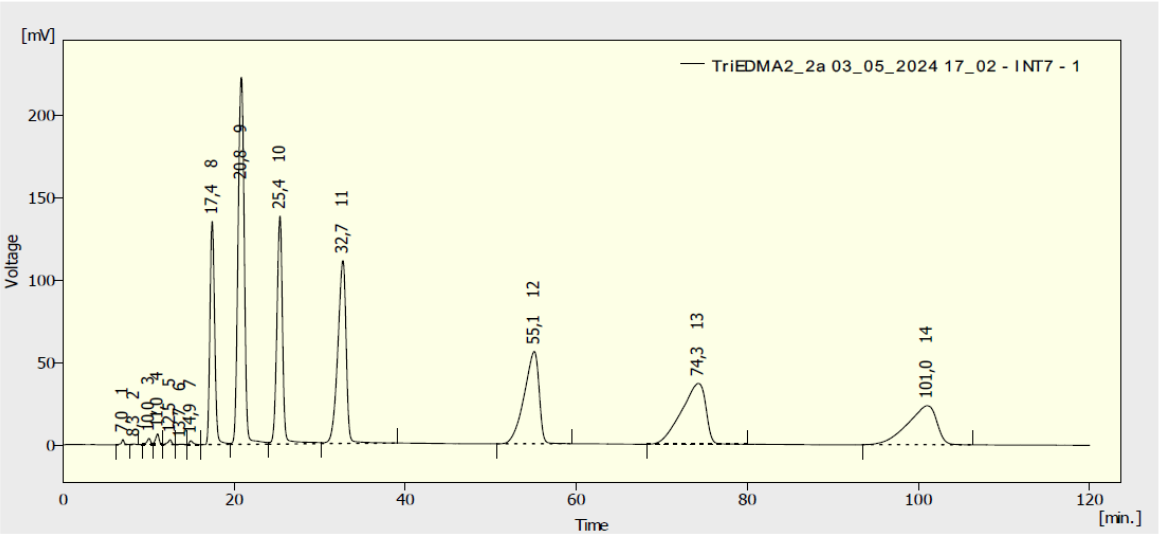

Figure 19: Chromatogram of alkylbenzenes separation on the TriEDMA monolithic column

As illustrated in **Figure 19**, the TriEDMA matrix demonstrates excellent resolution and high peak capacity. Despite the significantly longer retention times compared to TeEDMA, with the last analyte (peak 14) eluting at approximately 101 minutes, the early eluted peaks (1-4) maintain a well-defined morphology, confirming that longitudinal diffusion is effectively controlled by the monolithic structure. However, as retention increases, a slight fronting (tailing on the ascending side) becomes visible for the later eluting compounds. Nevertheless, the baseline remains stable, and the peaks are clearly integrable throughout the entire chromatogram. This indicates that the longitudinal diffusion is well contained by the monolithic structure.

The chromatographic profile confirms that the TriEDMA matrix process high surface homogeneity and efficient mass transfer properties regarding the kinetic performance of monolithic beds [37]. The consistent performance and thermodynamic stability ($R^2 = 0.9672$) of this column were decisive factors in selecting TriEDMA, along with TeEDMA, for further investigation in pharmaceutical applications, specifically for the analysis of APAP and its related compounds.

Aliphatic Series: 1,4 BUDMA

A significant change in chromatographic performance is observed when moving to the aliphatic cross-linkers series. Although the 1,4 BUDMA column maintained high thermodynamic consistency in the Martin Plot analysis ($R^2 = 0.9701$), the visual evidence from the chromatogram reveals a substantial decrease in efficiency.

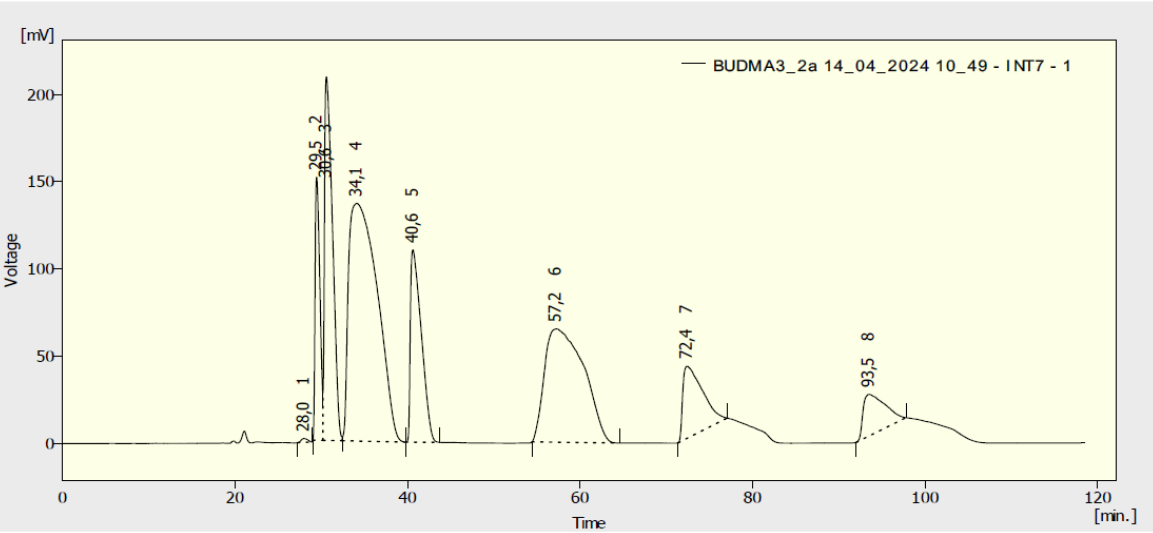

Figure 20: Chromatogram of alkylbenzenes separation on the 1,4 BUDMA monolithic column.

As shown in **Figure 20**, the peaks (numbered 2 to 8) exhibit significant peak broadening and a loss of symmetry compared to the glycol-based series. This phenomenon is primarily attributed to the presence of oversized macropores and a more heterogeneous pore size distribution, as previously suggested by the SEM micrographs. Such morphological irregularities enhance longitudinal dispersion and mass transfer resistance, leading to wider elution profiles [14].

Furthermore, the increased tortuosity of the polymer network in the aliphatic matrix likely hinders the ideal flow of the mobile phase, causing the analytes to follow inconsistent paths through the column [37]. These results demonstrate that while the chemical nature of the 1,4 BUDMA surface allows for a linear partition mechanism, its physical structure is less optimized for high-performance separation than the TeEDMA or TriEDMA counterparts.

Multifunctional acrylates: PETRA

The most critical chromatography performance was recorded for the PETRA column, synthesized with a highly branched multifunctional cross-linker. The experimental results provide a clear visual justification for the poor correlation coefficient ($R^2 = 0.6434$) observed in the thermodynamic study.

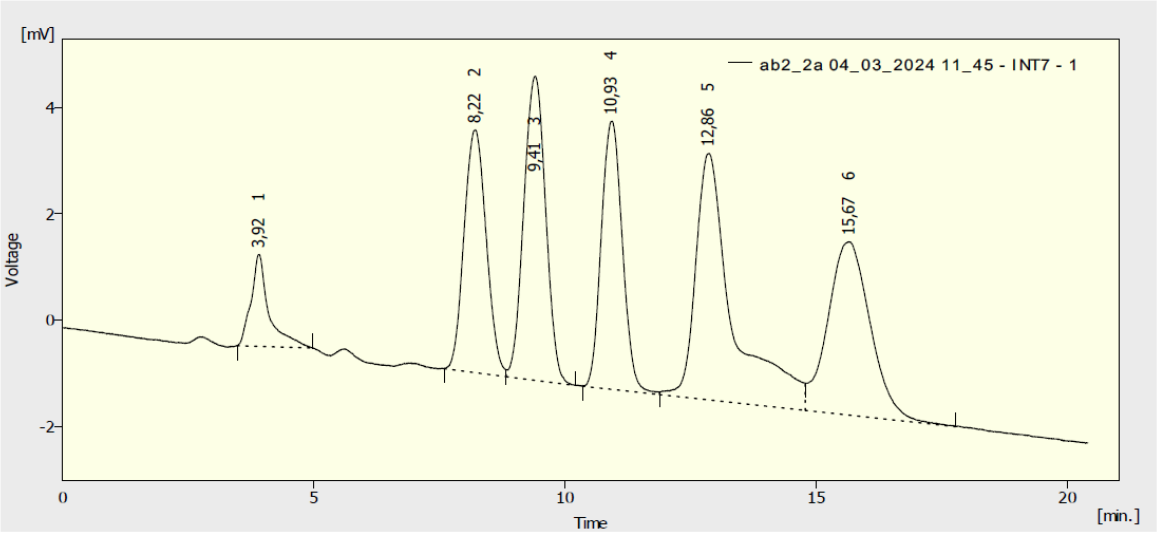

Figure 21: Chromatogram of alkylbenzenes separation on the PETRA monolithic column.

As shown in **Figure 21**, several critical issues emerge from the chromatographic profile. The separation appears incomplete, with only six detectable peaks; this suggests that the higher terms of the series are either co-eluting or suffering from excessive retention due to irreversible interactions within the complex polymer network. Furthermore, the significant drift in the baseline and the general peak deformation, particularly evident for the early eluted compounds, indicate a lack of structural integrity and an extremely slow equilibration process.

These observations confirm the inhomogeneous structure of this monolith [2]. The high degree of branching in the PETRA monomer likely leads to a tortuous and irregular pore distribution, which creates inconsistent flow paths and stagnant zones. Consequently, the mass transfer becomes unpredictable, and the ideal partition mechanism is completely disrupted. Structural heterogeneity is the primary cause of efficiency loss in monolithic beds, making this type of matrix unsuitable for high performance micro LC separation of small molecules [37].

Ultimately, the comparison between the thermodynamic data and the visual chromatographic profiles provides a definitive validation of the initial morphological hypotheses. While SEM analysis suggested superior architecture for the glycol-based matrices, these results confirm that such structural regularity translates directly into predictable elution patterns and high peak symmetry.

The TeEDMA and TriEDMA columns demonstrated that a well-connected globular network is the fundamental requirement for maintaining a consistent Reverse Phase partition

mechanism, minimizing the stagnant mass transfer zones that often plague monolith materials [37].

Interestingly, despite the increased peak broadening observed for the 1,4 BUDMA column, its high thermodynamic consistency remains a noteworthy result. This suggests that while physical morphology (macroporosity) affects kinetic efficiency, the chemical homogeneity of the surface still allows for a reliable and predictable retention mechanism. For this reason, 1,4 BUDMA was kept in consideration alongside the glycol-based series for the subsequent pharmaceutical applications.

Conversely, the performance of the PETRA column confirmed that extreme structural heterogeneity remains the primary limiting factor for efficiency in small molecule separations [2]. Having identified the most promising matrices, it is now essential to investigate their kinetic performance under increasing linear velocities through the study of Van Deemter plots.

4.4 Kinetic Evaluation and Van Deemter Analysis

The evaluation of the synthesized stationary phases was performed through the study of their kinetic profiles. The efficiency of each column was mathematically modeled using the Van Deemter equation. Specifically, the Height Equivalent to a Theoretical Plate (HETP) values were calculated using benzene as the probe solute, as it represented the first eluted peak of the homologous series. This approach allows for the deconvolution of the different physical phenomena contributing to peak broadening, represent by the A, B and C terms.

4.4.1 Preliminary Screening and Outlier Identification

Figure 22 shows the global comparison of all eight synthesized matrices. This initial overview is essential for identifying the overall performance trends across the different chemical compositions.

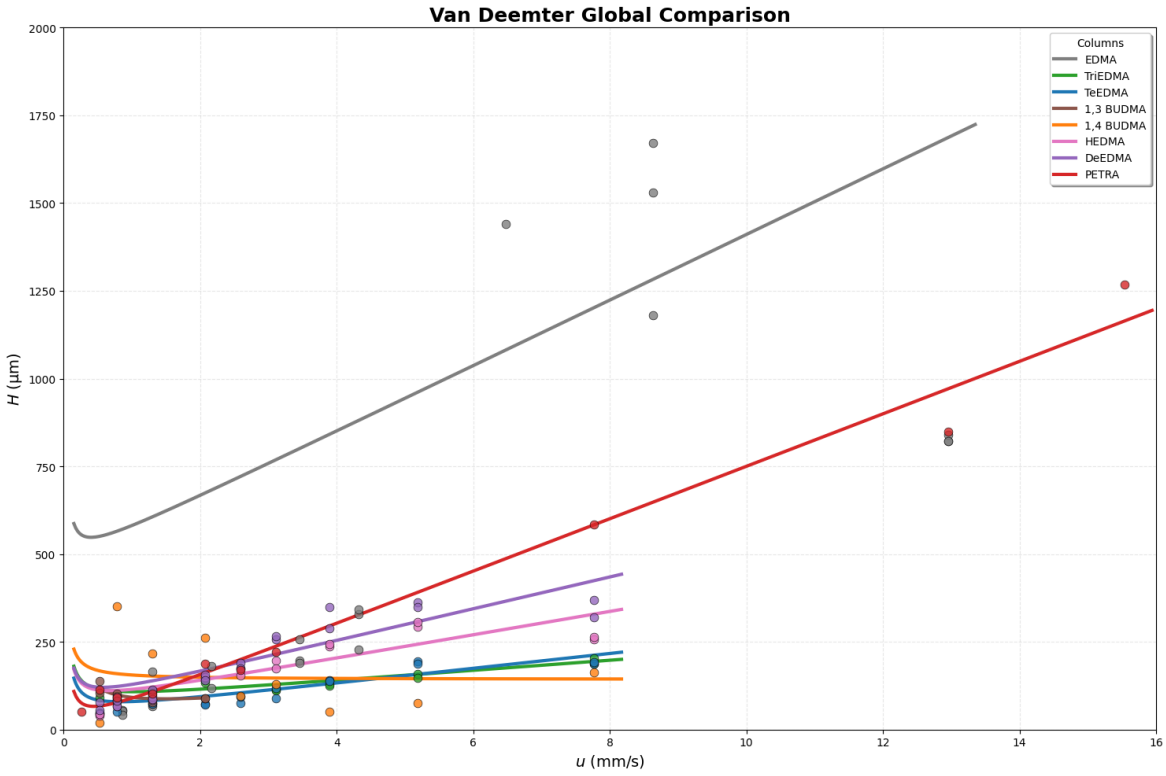

Figure 22: Global Van Deemter comparison including all synthesized matrices *(u in mm/s, H in µm).*

Preliminary results shown in **Figure 22** reveal a significant disparity in the performance of the different columns. Specifically, the matrices PETRA and EDMA act as clear outliers, showing H values that rapidly exceed 1000 µm. Such a steep slope in the Van Deemter plot is characteristic of a high C-term, indicating severe mass transfer resistance [4]. As summarized in **Table 7**, the calculated theoretical C-parameters for PETRA ($c = 74.85\ s$) and EDMA ($c = 93.57\ s$) are significantly higher than those of the other matrices. It should be noted that the Van Deemter curves do not include data for all flow rates across all columns; at higher flow velocities, the co-elution of alkylbenzenes occurred, preventing accurate plate height measurements. To ensure consistency, the analysis was focused on the first eluted peak (benzene). Furthermore, the kinetic parameters were derived through mathematical modeling (Python-based fitting), which in some instances may have slightly forced the trend to align with the theoretical model, particularly where experimental data points were limited. These values confirm that analyte diffusion is heavily hindered, likely due to a suboptimal or overly dense pore structure, which limits their applicability for high-speed separations.

***Table 7**: Van Deemter parameters and coefficients of determination (R^2) for the synthesized stationary phases Note: Parameters A, B and C were obtained through non-linear regression analyses of experimental data using the Van Deemter model ($H = A + B/u + Cu$). The R^2 values represent the goodness-of-fit, indicating the reliability of the calculated model for each specific architecture.*

Stationary Phase	A (μm)	B ($\mu m^2/s$)	C (s)	R^2
EDMA	472.83	0	93.63	0.13
TriEDMA	78.21	0	14.69	0.83
TeEDMA	43.41	0	21.45	0.86
1,3 BUDMA	36.88	37.98	16.95	0.43
1,4 BUDMA	142.55	13.00	0	0.0052
HEDMA	66.1	0	33.60	0.79
DEDMA	68.13	0	45.61	0.81
PETRA	0	14.62	74.86	0.98

To better appreciate the kinetic differences between the most performing matrices, it is necessary to exclude the outliers PETRA and EDMA from the visualization. As shown in **Figure 23**, the removal of these high-HETP profiles allows for a detailed zoom on the remaining six architectures, highlighting the performance of the methacrylate-based cross-linkers in the range below 450 µm.

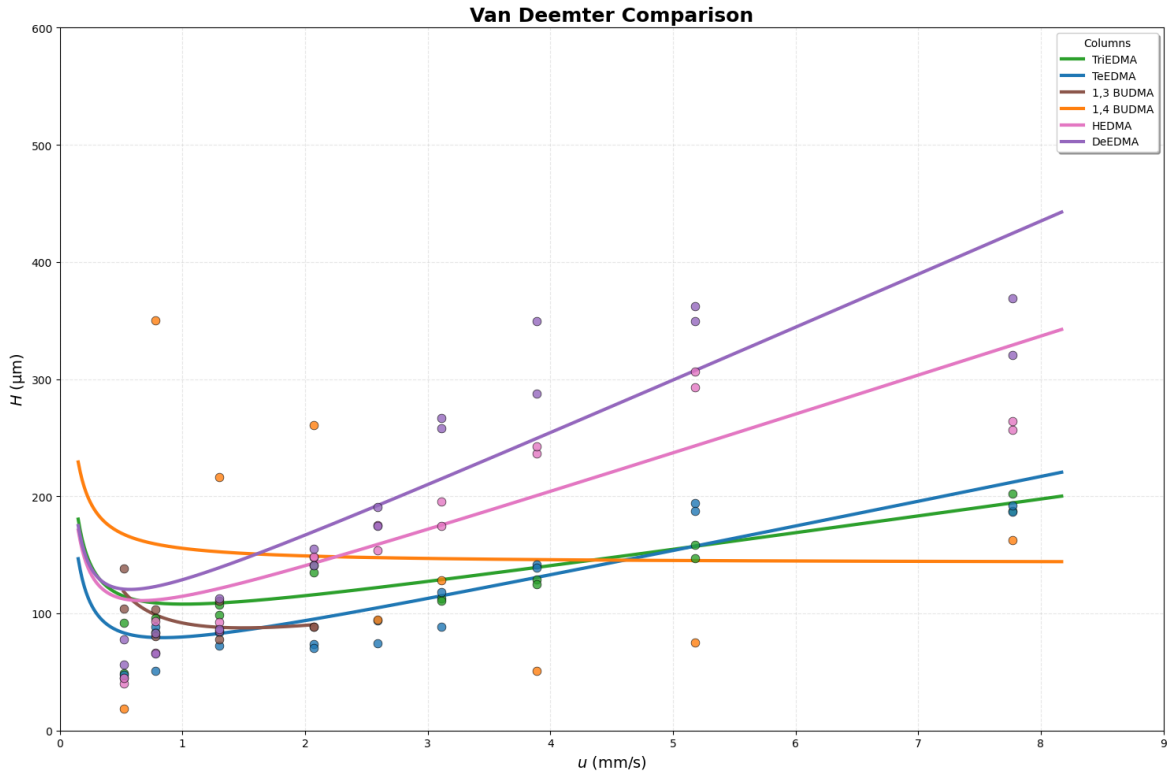

Figure 23: Focus on high-performing matrices. *The exclusion of outliers provides a clearer view of the kinetic competition at higher linear velocity*

In this refined comparison, it is evident that TeEDMA and TriEDMA maintain the lowest plate height across the entire velocity range. While their C-terms (21.43 and 14.69 s) are not the absolute lowest in the series, they represent a reliable balance between efficiency and structural stability.

Conversely, the BUDMA series (1,3 and 1,4 BUDMA) exhibits theoretical C-parameters near or equal to zero. Although a C-term of zero would ideally suggest a total absence of mass transfer resistance, an ideal condition in chromatography, in this context, it must be interpreted with caution. These values are a direct result of high scattering in the experimental data and the poor fitting quality, as evidenced by the very low or negative (R^2) values in **Table 7**, these near-zero values most likely stem from an insufficient fit of the non-linear Van Deemter curve to the experimental data. Specifically, the high scattering of the data points leads to a standard deviation of the C parameter that is significantly higher than the calculated value itself. Consequently, the parameter becomes statistically insignificant, and the regression software fails to provide a physically meaningful estimation of the mass transfer resistance for these specific columns.

When the experimental noise dominated the H vs u relationship, the regression model may fail to correctly partition the dispersion between A and C terms [4]. Therefore, for the BUDMA matrices, the near-zero C values likely reflect a lack of correlation rather than a physical absence of resistance, whereas for TeEDMA and TriEDMA, the values are mathematically solid and physically consistent with a well-developed macroporous scaffold, providing a reliable description of their kinetic performance [15].

4.4.2 Individual Performance and Model Validation

To further investigate the reliability of the kinetic parameters and the structural stability of the synthesized matrices, individual Van Deemter plots were analyzed for each high-efficiency column. This deconvolution is crucial to distinguish between columns that follow the theoretical model and those affected by significant experimental noise or structural non-ideality.

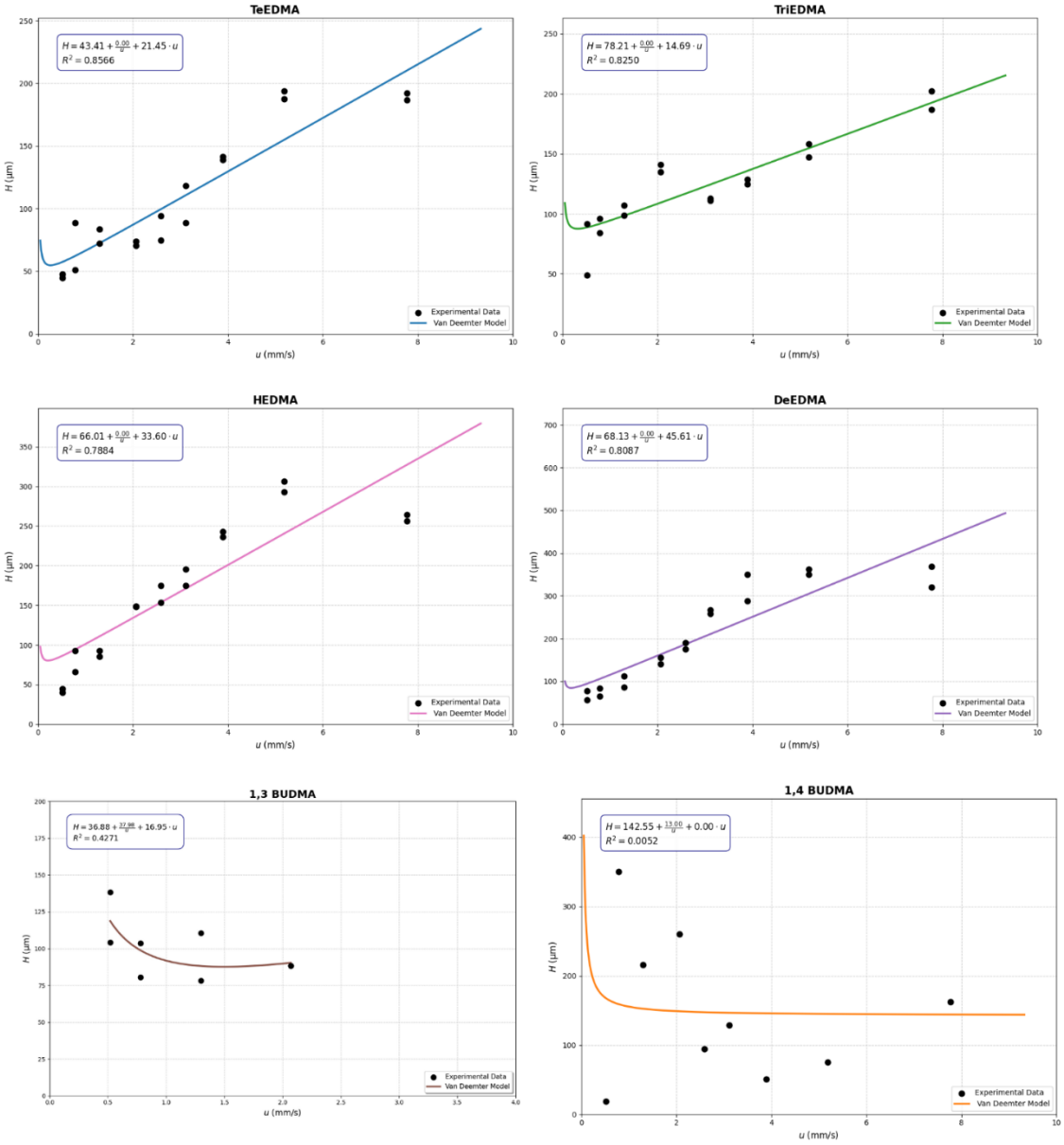

Figure 24: Individual Van Deemter regression plots for high-efficiency architectures. *The experimental data (points) are compared with theoretical fit (dashed line). Each plot reports the specific equation and the coefficient of determination (R^2).*

As shown in **Figure 24** the matrices TeEDMA and TriEDMA exhibit a strong correlation between experimental points and the theoretical model, with R^2 values exceeding 0.82. The progressive and coherent increase of the plate height (H) with the linear velocity (u) supports that the calculated C-terms are accurate physical descriptors of the mass transfer resistance. Such a well-defined kinetic profile is typical of monolithic structures where the cross-linker provides a rigid and accessible macroporous scaffold, minimizing peak broadening event at high flow rates [8].

In contrast, the individual plots for the BUDMA series are consistent with the lack of correlation previously suggested by the numerical data. The experimental points appear highly scattered, and the resulting flat trendlines do not represent an ideal mass transfer, but rather the inability of the model to fit the unstable kinetic behavior of these specific matrices.

This individual assessment suggests that the shorter chain length or the specific connectivity of the BUDMA cross-linkers might lead to structural non-homogeneity, a phenomenon often observed in organic monoliths during their development [7]. However, the superior performance and fitting quality of TeEDMA and TriEDMA demonstrate their potential for advanced applications.

4.4.3 Summary of Kinetic Performance

The comprehensive kinetic evaluation allows for a clear ranking of the synthesized stationary phases, highlighting how the chemical structure of the cross-linker dictates the final chromatographic performance. Based on experimental evidence and theoretical modeling, the matrices can be categorized as follows:

- High-Efficiency Architecture (TeEDMA and TriEDMA): these matrices emerged as the most promising candidates for advanced separations. Their ability to maintain low plate heights even at high linear velocities is a direct consequence of an optimized pore interconnectivity. A well-balanced cross-linking density provides the necessary structural rigidity to minimize mass transfer resistance (low C-term), allowing these columns to operate efficiently at flow rates that would typically compromise the resolution of traditional polymer monoliths.
- Intermediate Performance (HEDMA and DEDMA): these columns occupy an intermediate position in the ranking. While they demonstrate a stable and predictable Van Deemter profile, confirmed by satisfactory R^2 values, their C-parameters (33.58 and 45.58 s) indicate a greater resistance to mass transfer compared to the TeEDMA series. This suggests that while the matrices are structurally robust, their pore morphology is less favorable for efficient analyte transport at high flow rates.
- Non ideal and Inefficient Matrices (BUDMA, EDMA and PETRA): The BUDMA series, despite showing some low H values, suffered from high data scattering and poor model correlation, making the related monoliths unreliable for standard use. This instability, combined with the massive mass transfer resistance observed for

PETRA and EDMA (C>70 s), highlights the limitations of these specific chemistries. The homogeneity of the polymeric continuous rod is the key factor for efficiency [7]; in these cases, the shorter cross-linker chain or suboptimal polymerization likely led to a fragment or overly dense morphology that hinders diffusion.

In conclusion, the TeEDMA matrix represents the optimal balance between chemical architecture and kinetic efficiency. The results of this study suggest that increasing the number of methacrylate groups in the cross-linker is a successful strategy to create a robust scaffold capable of supporting high-speed separations without the dramatic loss of efficiency observed in less cross-linked or non-optimized architectures.

4.5 Separation of Acetaminophen and its metabolites: Retention study

4.5.1 Rational for column selection and experimental setup

Following the kinetic characterization described in the previous sections, a focused study was conducted to evaluate the practical applicability of the synthesized monoliths in the separation of real pharmaceutical compounds. For this purpose, three specific matrices were selected: TeEDMA, TriEDMA and 1,4 BUDMA.

The selection was based on a strategic comparison: TeEDMA and TriEDMA were chosen as the most promising candidates due to their superior kinetic performance and high efficiency observed in the Van Deemter analysis, while 1,4 BUDMA was included to further investigate the impact of a shorter and more flexible cross-linker chain on the retention of polar analytes [38].

To ensure maximum structural stability and bed homogeneity during these prolonged isocratic tests, new columns were synthesized with optimized lengths (ranging from 180 to 190 mm). This re-synthesis was crucial to minimize potential "channeling" effects and to verify the reproducibility of the polymerization process, as the internal morphology of the continuous rod is highly sensitive to small variations in the synthesis conditions [8]. The geometric dimensions of these newly synthesized columns, which served as the basis for all subsequent hydrodynamic and porosity calculations, are summarized in **Table 8**.

Table 8: Geometric dimensions of the re-synthesized monolithic columns. *Note: The geometric volume was calculated as* $V_{geom} = \pi \cdot r^2 \cdot L$.

Column	Column Length (L, mm)	Inner Diameter (ID, mm)	Geometric Volume ($V_{geom}, \mu L$)
TeEDMA	180	0.32	14.48
TriEDMA	190	0.32	15.28
1,4 BUDMA	185	0.32	14.88

The target analyte chosen for this study is APAP, along with three of its primary polar conjugates: acetaminophen-cysteine (ACYS), acetaminophen-N-acetylcisteine (ANAC) and acetaminophen-glutathione (ASG). These compounds represent a significant analytical challenge due to their high hydrophilicity. As noted in the initial experimental assessment, providing data on the retention behavior of these metabolites on polymethacrylate monoliths represents a novel contribution to the field, as such data are currently scarce in the specialized literature regarding organic monolithic supports.

Although the experimental conditions tested did not lead to a complete baseline separation suitable for a standardized pharmaceutical method, the results are valuable as an exploratory study aimed at assessing whether the synthesized monolithic columns could function under Hydrophilic Interaction Liquid Chromatography (HILIC) conditions, while also providing insight into their surface chemistry and potential for such applications, where rapid mass transfer is a key requirement [4].

In this context, the observed retention behavior suggests a dual-mode mechanism, where the columns transition from Reversed-Phase (RP) to HILIC depending on the mobile phase composition. This bimodal character is well-documented for methacrylate-based monoliths [39]. This versatility could allow for the interaction with both the hydrophobic core of the parent drug (APAP) and the highly polar moieties of its conjugates (ACYS, ANAC, ASG), confirming the potential of these materials for multidimensional or multi-mode chromatographic applications.

4.5.2 Evaluation of Retention behavior and HILIC mechanism

Structural Characterization and the Toluene Paradox

The initial hydrodynamic characterization of the monolithic beds was performed by determining the dead time (t_m) using toluene as a non-retained marker. This parameter allowed for the calculation of the dead volume (V_m) and the total porosity (ε), defining the physical and structural baseline of the synthesized columns. These parameters, which represent the fundamental hydrodynamic properties of the matrices, are summarized in **Table 9**.

Table 9: Hydrodynamic parameters of the synthesized monoliths (Toluene-based). Mobile phase: acetonitrile/water 95/5; flow: 10 µL/min

Column	t_m(min)	V_m (μL)	Total Porosity(ε)
TeEDMA	1.11	11.1	0.767
TriEDMA	0.967	19.34	1.266
1,4 BUDMA	4.15	83	5.578

However, a critical evaluation of these preliminary results indicated that toluene is not an ideal dead-time marker for the synthesized matrices. In a physically consistent monolithic system, the total porosity (ε) must be mathematically lower than 1. For the 1,4-BUDMA and TriEDMA columns, the calculated porosity values using toluene exceeded this theoretical limit. This discrepancy (or 'porosity anomaly') suggests that toluene undergoes secondary interactions with the polymeric skeleton, likely through a Reversed-Phase (RP) mechanism facilitated by the hydrophobic 1,4-butanediyl or oxyethylene moieties [8]. Consequently, the elution volume of toluene in these specific matrices reflects a combination of the interstitial volume and a degree of chemical retention, leading to an overestimation of the column porosity.

In contrast, the TeEDMA column, which possesses a higher density of oxygen atoms and a more pronounced hydrophilic character, yielded a physically consistent porosity value ($\varepsilon < 1$). This indicates that on the TeEDMA surface, the HILIC-like environment effectively suppresses the hydrophobic adsorption of toluene, allowing it to behave more closely to an ideal unretained probe.

Refinement of the Dead Volume: The Thiourea Extrapolation Method

To ensure the accuracy of the retention factors (k) for the subsequent pharmaceutical study, it was necessary to adopt a more robust approach for the 1,4-BUDMA and TriEDMA columns. Thiourea was selected as an alternative polar probe. To account for any potential HILIC-mode partitioning of thiourea itself at high organic concentrations, the dead time (t_m) was determined by extrapolating its retention times to a 100% aqueous mobile phase. Under these conditions, the HILIC mechanism is effectively suppressed [40], and the probe elutes based purely on the accessible interstitial volume This correct procedure, summarized in **Table 10**, provided the reliable hydrodynamic baseline necessary for the final calculation of the retention factors.

Table 10: Corrected dead time (t_m), volume (V_m) and porosity (ε) derived from thiourea extrapolation.

Column	t_m(min)	V_m (μL)	Total Porosity(ε)
1,4 BUDMA	0.683	13.66	0.92
TriEDMA	0.531	10.62	0.695

Comparative analysis of retention mechanisms and structural correlations

The experimental results for the retention of APAP are presented in **Figure 25**, which illustrates the retention profiles as a function of the organic modifier percentage, and **Errore. L'origine riferimento non è stata trovata.** provides a comparative overview of the retention factors (k) at the highest acetonitrile concentration (90% ACN) for APAP and its conjugates.

These data provide a comparative overview of the retention factors, highlighting a clear divergence in the behavior of the synthesized matrices. For the TeEDMA (Figure 25a) and 1,4-BUDMA (Figure 25c) matrices retention increases as the acetonitrile (ACN) concentration increases beyond 70%. This behavior is a hallmark of the Hydrophilic Interaction Liquid Chromatography (HILIC) mechanism, in which polar analytes distribute into a water-rich layer adsorbed on the polar monolithic surface [9].

In striking contrast, the TriEDMA matrix (Figure 25b) displayed a significantly different profile. Throughout the entire range of mobile phase compositions, the retention remains

remarkably low, with $\log k$ values consistently staying below zero. Unlike the other two columns, TriEDMA does not exhibit a dominant HILIC upward trend at high organic percentages; instead, it shows a nearly flat profile with a slight downward slope.

This distinct behavior suggests that the ethylene oxide chain length and the specific density of the oxygen atoms in this matrix are insufficient to establish a stable, hydrated stagnant layer. Consequently, the HILIC partition mechanism is not effectively triggered, and the analytes elute almost unretained, influenced only by very weak residual interactions. This comparison highlights that while TriEDMA showed excellent kinetic properties in the Van Deemter study, it lacks the necessary surface hydrophilicity for the effective separation of polar APAP metabolites.

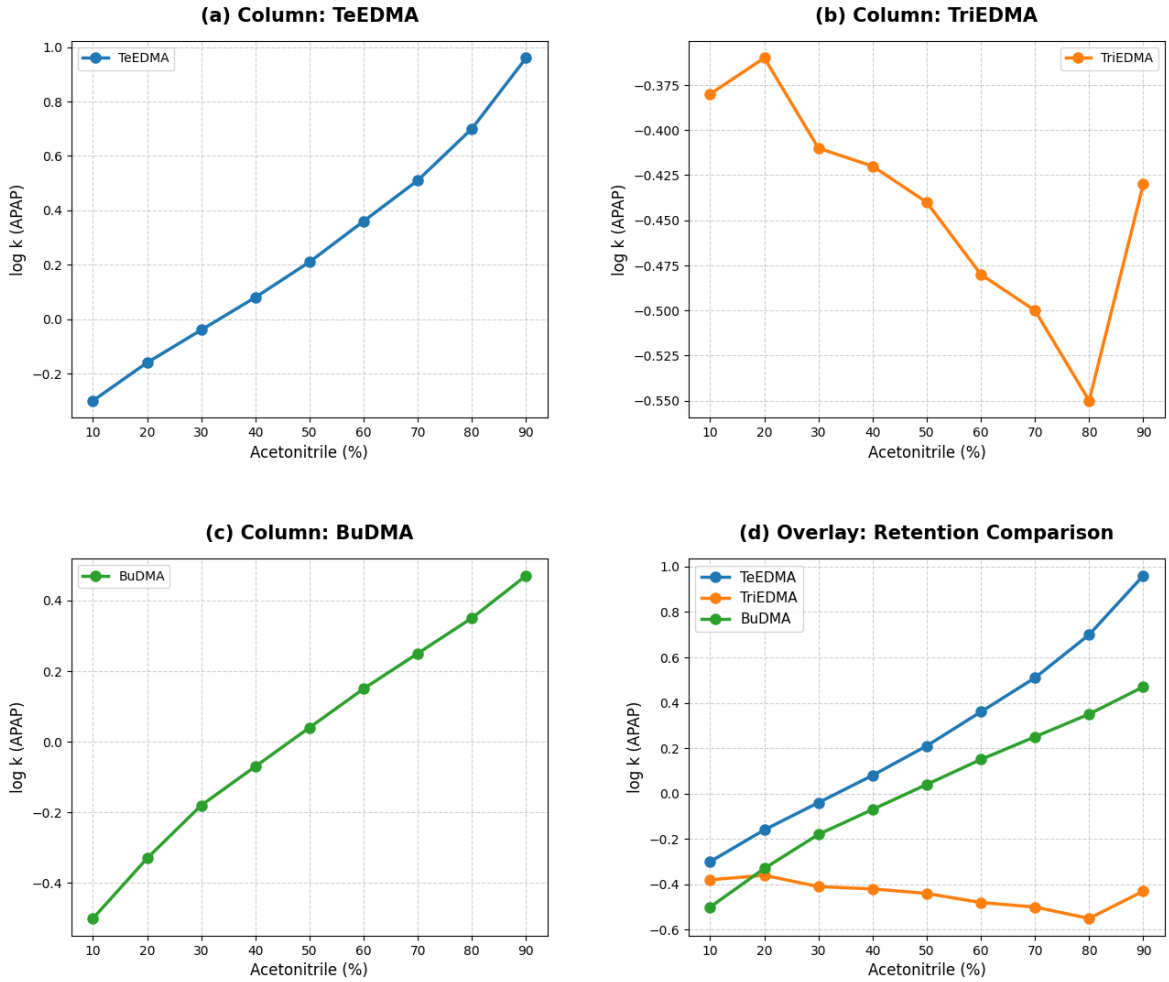

Figure 25: Retention profile of APAP on TeEDMA, TriEDMA and 1,4-BUDMA monolithic columns. *Plots (a), (b) and (c) show the individual trends for $\log k$ vs $Acetonitrile$ (%), while plot (d) presents the comparative overlay. The exponential increase at high ACN percentages confirms the HILIC retention mechanism.*

Comparative analysis of APAP and Metabolite Retention

The comparative retention study with mobile phase at 90% ACN highlights significant differences in how the monolithic matrices interact with the parent drug versus its polar conjugates (**Errore. L'origine riferimento non è stata trovata.**).

Concerning APAP, the TeEDMA-based monolith achieved the highest retention factor ($k = 9.17$), significantly outperforming both 1,4 BUDMA ($k = 2.96$) and TriEDMA ($k = 0.37$). This superior performance confirms that the four oxyethylene units in the TeEDMA cross-linker are essential for creating a sufficiently dense hydrophilic environment to partition small polar molecules effectively [41].

The subsequent analysis of the metabolite series (ACYS, ANAC, and ASG) revealed a more complex scenario. On the TeEDMA column, the metabolites showed a significant decrease in retention ($k \approx 5.40$) compared to the parent drug. Conversely, the 1,4-BUDMA matrix exhibited a stronger affinity for the conjugates ($k \approx 8.50$). However, a common bioanalytical limitation emerged for both matrices: despite the satisfactory retention, the three metabolites were not resolved from each other, showing nearly identical k values. This indicates that while the retention trend for metabolites differs slightly from that of APAP, they still suffer from co-elution, preventing their individual separation.

It is important to note that, as suggested by preliminary data evaluation, the experimental points at the highest acetonitrile concentration (90% ACN) might represent potential outliers. Under these extreme HILIC conditions, the stability of the stagnant water layer can be compromised, potentially affecting the reproducibility of the partition and leading to fluctuations in the measured retention factors.

Table 11: Comparison of retention factors (k) at 90% Acetonitrile of APAP and its conjugates

	TeEDMA	TriEDMA	1,4 BUDMA
APAP	9.17	0.37	2.96
ACYS	5.40	0.26	8.59
ANAC	5.38	0.25	8.55
ASG	5.38	0.24	8.44

In conclusion, these results demonstrate that while the synthesized monolithic matrices successfully establish a HILIC environment capable of retaining highly polar drug conjugates, the delicate balance between hydrophilic partitioning and residual hydrophobic interactions, driven by the cross-linker architecture, is the determining factor for achieving effective chromatographic selectivity.

5. Conclusions and Future Perspectives

The research presented in this thesis demonstrates that the chemical architecture of oxyethylene-based cross-linkers is a fundamental factor in determining both the physical structure and the chromatographic performance of polymethacrylate-based monoliths for HILIC applications. The comparative study conducted on TeEDMA, TriEDMA, and 1,4 BUDMA matrices revealed that the length and flexibility of the cross-linker chain directly influence the formation of the hydrophilic stagnant layer necessary for the partitioning of polar analytes.

Among the synthesized materials, TeEDMA emerged as the most promising candidate, showing superior kinetic efficiency and a robust HILIC mechanism driven by its high oxygen density. In contrast, 1,4 BUDMA exhibited a complex mixed-mode behavior, where HILIC interactions were accompanied by residual hydrophobic effects, while TriEDMA failed to establish a stable hydrophilic environment, showing a prevalent Reversed-Phase trend for the target analytes.

A significant methodological result of this study was the resolution of the hydrodynamic characterization issues. By recognizing that standard markers like toluene are subject to hydrophobic retention on these polymer skeletons, a more rigorous approach using thiourea extrapolation to pure water conditions was successfully implemented. This ensured that the calculated retention factors for acetaminophen and its metabolites were based on a physically accurate interstitial volume, effectively suppressing any HILIC partitioning of the dead time marker itself.

While the current isocratic conditions demonstrated high retentivity on TeEDMA and 1,4-BUDMA, a major bioanalytical challenge remains the co-elution of the highly polar APAP metabolites. The experimental data confirmed that while these matrices successfully trap the conjugates, they currently lack the specific selectivity required to resolve them individually. Furthermore, the analysis at extreme organic concentrations (90% ACN) suggested the presence of potential outliers, likely due to the limited stability of the hydrated layer under such conditions.

Future perspectives for this research will focus on leveraging the high efficiency of the TeEDMA matrix while enhancing its selectivity through the optimization of mobile phase parameters, such as pH and ionic strength, or the implementation of gradient elution strategies. Additionally, the incorporation of charged functional monomers onto the

TeEDMA-like backbone could be explored to introduce ion-exchange interactions, potentially resolving the co-elution issue.

In conclusion, this study confirms that polymethacrylate monoliths, particularly the TeEDMA architecture, are effective and versatile platforms for the rapid analysis of polar pharmaceutical compounds, providing a solid foundation for the development of advanced micro-HPLC clinical applications.

6. Abbreviations

1,3-BUDMA: 1,3-Butanediol dimethacrylate

1,4-BUDMA: 1,4-Butanediol dimethacrylate

A: Methylene group selectivity (Martin plot slope)

ACN: Acetonitrile

ACYS: Acetaminophen-cysteine

ADHD: Attention-Deficit/Hyperactivity Disorder

AIBN: 2,2'-Azobis(2-methylpropionitrile)

AM404: N-arachidonoylaminophenol

ANAC: Acetaminophen-N-acetylcysteine

APAP: Acetaminophen (N-acetyl-p-aminophenol)

APAP-AD: Acetaminophen-protein adducts

APAP-gluc: Acetaminophen glucuronide

ASG: Acetaminophen-glutathione

ATP: Adenosine Triphosphate

B: Phenyl group interaction constant (Martin plot intercept)

CNS: Central Nervous System

COX: Cyclooxygenase

CYP450: Cytochrome P450

DeEDMA: 1,10-Decanediol dimethacrylate

DNA: Deoxyribonucleic Acid

EDMA: Ethylene glycol dimethacrylate

EtOH: Ethanol

F: Flow rate

FAAH: Fatty Acid Amide Hydrolase

GSH: Reduced Glutathione

GST: Glutathione S-transferase

H (or HETP): Height Equivalent to a Theoretical Plate

HCl: Hydrochloric acid

HEDMA: 1,6-Hexanediol dimethacrylate

HILIC: Hydrophilic Interaction Liquid Chromatography

HPLC: High-Performance Liquid Chromatography

k: Retention factor

K_0: Specific permeability

L: Effective length of the monolithic bed

LC-MS/MS: Liquid Chromatography-tandem Mass Spectrometry

LMA: Lauryl methacrylate

micro-HPLC: Capillary High-Performance Liquid Chromatography

MPT: Mitochondrial Permeability Transition

mtDNA: Mitochondrial DNA

N: Number of Theoretical Plates

NAC: N-acetylcysteine

NAPQI: N-acetyl-p-benzoquinone imine

NaOH: Sodium hydroxide

NSAIDs: Non-Steroidal Anti-Inflammatory Drugs

PAPS: 3'-phosphoadenosine-5'-phosphosulfate

PETRA: Pentaerythritol triacrylate

PG / PGE: Prostaglandin / Prostaglandin E

PhDMA: 1,4-Phenylene dimethacrylate

POX: Peroxidase

SAR: Structure-Activity Relationship

SEM: Scanning Electron MicroscopySi-OH: Silanol groups

SULT: Sulfotransferase

t_0: Column void time (dead time)

t_R : Retention time

TeEDMA: Tetraethylene glycol dimethacrylate

THU: Thiourea (Tiourea)

TriEDMA: Triethylene glycol dimethacrylate

TRPV1: Transient Receptor Potential Vanilloid 1

u: Linear velocity of the mobile phase

UGT: UDP-glucuronosyltransferase

VAMS: Volumetric Absorptive Microsampling

V_m: Dead volume (void volume)

ε (epsilon): Total porosity

Φ: Volume fraction of organic modifier in the mobile phase

$w_{0,5}$: Peak width at half-height

7. References

1. Svec F. Porous polymer monoliths: amazingly wide variety of techniques enabling their preparation. *J Chromatogr A*. 2010;1217(6):902-924. doi:10.1016/j.chroma.2009.09.073

2. Vlakh EG, Tennikova TB. Applications of polymethacrylate-based monoliths in high-performance liquid chromatography. *J Chromatogr A*. 2009;1216(13):2637-2650. doi:10.1016/j.chroma.2008.09.090

3. Acquah C, Moy CKS, Danquah MK, Ongkudon CM. Development and characteristics of polymer monoliths for advanced LC bioscreening applications: A review. *J Chromatogr B*. 2016;1015-1016:121-134. doi:10.1016/j.jchromb.2016.02.016

4. Guiochon G. Monolithic columns in high-performance liquid chromatography. *J Chromatogr A*. 2007;1168(1):101-168. doi:10.1016/j.chroma.2007.05.090

5. Souza ID, Queiroz MEC. Organic-silica hybrid monolithic sorbents for sample preparation techniques: A review on advances in synthesis, characterization, and applications. *J Chromatogr A*. 2024;1713:464518. doi:10.1016/j.chroma.2023.464518

6. Nischang I, Teasdale I, Brüggemann O. Porous polymer monoliths for small molecule separations: advancements and limitations. *Anal Bioanal Chem*. Published online 2010. doi:10.1007/s00216-010-4579-6

7. Svec F, Fréchet JMJ. Modified poly(glycidyl metharylate-co-ethylene dimethacrylate) continuous rod columns for preparative-scale ion-exchange chromatography of proteins. *J Chromatogr A*. 1995;702(1):89-95. doi:10.1016/0021-9673(94)01021-6

8. Urban J, Jandera P. Polymethacrylate monolithic columns for capillary liquid chromatography. *J Sep Sci*. Published online 2008. doi:10.1002/jssc.200800182

9. Jandera P, Staňková M, Škeříková V, Urban J. Cross-linker effects on the separation efficiency on (poly)methacrylate capillary monolithic columns. Part I. Reversed-phase liquid chromatography. *J Chromatogr A*. 2013;1274:97-106. doi:10.1016/j.chroma.2012.12.003

10. Aggarwal P, Tolley HD, Lee ML. Monolithic bed structure for capillary liquid chromatography. *J Chromatogr A*. 2012;1219:1-14. doi:10.1016/j.chroma.2011.10.083

11. Lee D, Svec F, Fréchet JMJ. Photopolymerized monolithic capillary columns for rapid micro high-performance liquid chromatographic separation of proteins. *J Chromatogr A*. 2004;1051(1):53-60. doi:10.1016/j.chroma.2004.04.047

12. Viklund C, Svec F, Fréchet JMJ, Irgum K. Monolithic, “Molded”, Porous Materials with High Flow Characteristics for Separations, Catalysis, or Solid-Phase Chemistry: Control of Porous Properties during Polymerization. *Chem Mater*. 1996;8(3):744-750. doi:10.1021/cm950437j

13. Eeltink S, Herrero-Martinez JM, Rozing GP, Schoenmakers PJ, Kok WTh. Tailoring the Morphology of Methacrylate Ester-Based Monoliths for Optimum Efficiency in Liquid Chromatography. *Anal Chem*. 2005;77(22):7342-7347. doi:10.1021/ac051093b

14. Poppe H. Some reflections on speed and efficiency of modern chromatographic methods. *J Chromatogr A*. 1997;778(1):3-21. doi:10.1016/S0021-9673(97)00376-2

15. Staňková M, Jandera P, Škeříková V, Urban J. Cross-linker effects on the separation efficiency on (poly)methacrylate capillary monolithic columns. Part II. Aqueous normal-phase liquid chromatography. *J Chromatogr A*. 2013;1289:47-57. doi:10.1016/j.chroma.2013.03.025

16. Ayoub SS. Paracetamol (acetaminophen): A familiar drug with an unexplained mechanism of action. *Temp Multidiscip Biomed J*. 8(4):351-371. doi:10.1080/23328940.2021.1886392

17. Bertolini A, Ferrari A, Ottani A, Guerzoni S, Tacchi R, Leone S. Paracetamol: new vistas of an old drug. *CNS Drug Rev*. 2006;12(3-4):250-275. doi:10.1111/j.1527-3458.2006.00250.x

18. Brune K, Renner B, Tiegs G. Acetaminophen/paracetamol: A history of errors, failures and false decisions. *Eur J Pain*. Published online 2014. doi:10.1002/ejp.621

19. Vane JR, Botting RM. Anti-inflammatory drugs and their mechanism of action. *Inflamm Res*. 1998;47(2):78-87. doi:10.1007/s000110050284

20. McGovern MC, Glasgow JFT, Stewart MC. Reye's syndrome and aspirin: lest we forget. *BMJ*. 2001;322(7302):1591-1592. doi:10.1136/bmj.322.7302.1591

21. Ouellet M, Percival MD. Mechanism of Acetaminophen Inhibition of Cyclooxygenase Isoforms. *Arch Biochem Biophys*. 2001;387(2):273-280. doi:10.1006/abbi.2000.2232

22. Bauer AZ, Swan SH, Kriebel D, et al. Paracetamol use during pregnancy — a call for precautionary action. *Nat Rev Endocrinol*. 2021;17(12):757-766. doi:10.1038/s41574-021-00553-7

23. Chandrasekharan NV, Dai H, Roos KLT, et al. COX-3, a cyclooxygenase-1 variant inhibited by acetaminophen and other analgesic/antipyretic drugs: Cloning, structure, and expression. *Proc Natl Acad Sci U S A*. 2002;99(21):13926-13931. doi:10.1073/pnas.162468699

24. Schwab JM, Schluesener HJ, Meyermann R, Serhan CN. COX-3 the enzyme and the concept: steps towards highly specialized pathways and precision therapeutics? *Prostaglandins Leukot Essent Fatty Acids*. 2003;69(5):339-343. doi:10.1016/j.plefa.2003.07.003

25. Hodgman MJ, Garrard AR. A Review of Acetaminophen Poisoning. *Crit Care Clin*. Published online 2012. doi:10.1016/j.ccc.2012.07.006

26. McGill MR, Jaeschke H. METABOLISM AND DISPOSITION OF ACETAMINOPHEN: RECENT ADVANCES IN RELATION TO HEPATOTOXICITY AND DIAGNOSIS. *Pharm Res*. 2013;30(9):2174-2187. doi:10.1007/s11095-013-1007-6

27. Mazaleuskaya LL, Sangkuhl K, Thorn CF, FitzGerald GA, Altman RB, Klein TE. PharmGKB summary: Pathways of acetaminophen metabolism at the therapeutic versus toxic doses. *Pharmacogenet Genomics*. 2015;25(8):416-426. doi:10.1097/FPC.0000000000000150

28. Hinson JA, Roberts DW, James LP. Mechanisms of Acetaminophen-Induced Liver Necrosis. *Handb Exp Pharmacol*. 2010;(196):369-405. doi:10.1007/978-3-642-00663-0_12

29. Rumack BH, Matthew H. Acetaminophen Poisoning and Toxicity. *Pediatrics*. 1975;55(6):871-876. doi:10.1542/peds.55.6.871

30. Vanova J, Malinak D, Andrys R, et al. Optimization of gradient reversed phase high performance liquid chromatography analysis of acetaminophen oxidation metabolites using linear and non-linear retention model. *J Chromatogr A*. 2022;1669:462956. doi:10.1016/j.chroma.2022.462956

31. Delahaye L, Baerdemaeker LD, Stove CP. Determination of paracetamol and its metabolites via LC-MS/MS in dried blood volumetric absorptive microsamples: A tool for pharmacokinetic studies. *J Pharm Biomed Anal*. 2021;206:114361. doi:10.1016/j.jpba.2021.114361

32. Hewavitharana AK, Lee S, Dawson PA, Markovich D, Shaw PN. Development of an HPLC–MS/MS method for the selective determination of paracetamol metabolites in mouse urine. *Anal Biochem*. 2008;374(1):106-111. doi:10.1016/j.ab.2007.11.011

33. Svec F. Quest for organic polymer-based monolithic columns affording enhanced efficiency in high performance liquid chromatography separations of small molecules in isocratic mode. *J Chromatogr A*. 2012;1228:250-262. doi:10.1016/j.chroma.2011.07.019

34. Urban J, Moravcová D, Jandera P. A model of flow-through pore formation in methacrylate ester-based monolithic columns. *J Sep Sci*. Published online 2006. doi:10.1002/jssc.200500457

35. Nesterenko EP, Nesterenko PN, Connolly D, Lacroix F, Paull B. Micro-bore titanium housed polymer monoliths for reversed-phase liquid chromatography of small molecules. *J Chromatogr A*. 2010;1217(14):2138-2146. doi:10.1016/j.chroma.2010.02.007

36. Martin AJP, Synge RLM. A new form of chromatogram employing two liquid phases. *Biochem J*. 1941;35(12):1358-1368. doi:10.1042/bj0351358

37. *Fundamentals of Preparative and Nonlinear Chromatography*. (2nd Edition, 2006) by G. Guiochon, A. Felinger, D.G. Shirazi, and A.M. Katti

38. Jandera P, Hájek T, Staňková M. Monolithic and core–shell columns in comprehensive two-dimensional HPLC: a review. *Anal Bioanal Chem*. Published online 2014. doi:10.1007/s00216-014-8147-3

39. Jandera P. Stationary phases for hydrophilic interaction chromatography, their characterization and implementation into multidimensional chromatography concepts. *J Sep Sci*. Published online 2008. doi:10.1002/jssc.200800051

40. Hemström P, Irgum K. Hydrophilic interaction chromatography. *J Sep Sci*. Published online 2006. doi:10.1002/jssc.200600199

41. Buszewski B, Noga S. Hydrophilic interaction liquid chromatography (HILIC)—a powerful separation technique. *Anal Bioanal Chem*. Published online 2011. doi:10.1007/s00216-011-5308-5